

Measurement report: Secondary Impact of cloud processes on secondary organic aerosols at a forested mountain site in southeastern China

5 Zijun Zhang^{1,2}, Weiqi Xu^{1,*}, Yi Zhang^{1,2}, Wei Zhou¹, Xiangyu Xu^{1,2}, Aodong Du^{1,2}, Yinzhou Zhang¹,
Hongqin Qiao³, Ye Kuang³, Xiaole Pan¹, Zifa Wang^{1,2}, Xueling Cheng¹, Lanzhong Liu⁴, Qingyan Fu⁵,
Douglas R. Worsnop⁶, Jie Li¹, Yele Sun^{1,2,*}

¹State Key Laboratory of Atmospheric Boundary Layer Physics and Atmospheric Chemistry, Institute of Atmospheric Physics, Chinese Academy of Sciences, Beijing 100029, China

²College of Earth and Planetary Sciences, University of Chinese Academy of Sciences, Beijing 100049, China

10 ³Institute for Environmental and Climate Research, Jinan University, Guangzhou 511143, China

⁴Shanghuang ~~Atmospheric Boundary Layer and Eco-Environment~~ Environmental Observatory, ~~Institute of Atmospheric Physics~~, Chinese Academy of Sciences, Jinhua 321203, China

⁵Shanghai Environmental Monitoring Center, Shanghai 200235, China

⁶Aerodyne Research Inc., Billerica, Massachusetts 01821, United States

15 *Correspondence to:* Weiqi Xu (xuweiqi@mail.iap.ac.cn), Yele Sun (sunyele@mail.iap.ac.cn)

Abstract. Aerosol particles play ~~erueialcritical~~ crucial roles in ~~both~~ climate ~~dynamics~~ and human health. However, ~~there remains a significant gap in our understanding of~~ aerosol composition and evolution, particularly ~~regarding~~ secondary organic aerosols (SOA), and ~~theirs~~ their interaction with clouds in high-altitude background areas in China: ~~remain less understood~~. Here we conducted real-time measurements of submicron aerosols (PM₁) using aerosol mass spectrometers at a forested mountain site (1128 m a.s.l.) in southeastern China in November 2022. ~~Our results revealed that organic~~ The average ($\pm 1\sigma$) PM₁ mass concentration was $4.45 \pm 6.51 \mu\text{g m}^{-3}$, which was ubiquitously lower than those at other mountain sites in China. Organic aerosol (OA) constituted ~~a substantial portion~~ the largest fraction of PM₁ (41.1 %), with the OA being primarily of ~~42.9 %~~ 42.9 % and was dominantly secondary ~~origin~~, as ~~evidenced~~ indicated by ~~athe~~ high oxygen-to-carbon (O/C) ratio (0.85–0.96) and carbon oxidation state (0.21–0.49). Back trajectory analysis revealed that higher concentrations of PM₁ were mainly associated with the transport from the western and southwestern regions. Notably, the remarkably enhanced PM₁ concentrations observed during daytime on cloudless days were identified to be likely produced from cloud evaporation. Positive matrix factorization resolved two distinct ~~SOA/OOA~~ factors, i.e., less oxidized oxygenated OA (LO-OOA) and more oxidized OOA (MO-OOA). ~~Interestingly, While~~ MO-OOA was scavenged efficiently during cloud events, ~~while~~ cloud evaporation ~~contributed significantly~~ was found to release a significant amount of LO-OOA. ~~The ratio from air mass transported from polluted regions. The distinct increase of OA/ ΔCO increased/ ΔCO (CO after subtracting the background level) with~~ athe decrease ~~in the~~ of O/C ratio, ~~suggesting~~ during the cloud evaporative period further demonstrates that OA ~~remaining~~ remained in cloud droplets are generally maintained in a moderate oxidation state. ~~Furthermore, our results indicated~~ Moreover, organic nitrates were also estimated and showed a higher contribution ~~of organic nitrates~~ to the total

20
25
30

nitrate during ~~the cloudy periods~~ period (27 %) ~~compared to evaporative periods (3 %)~~. Notably, a substantial contribution of ~~nitrate in PM₁ (20.9 %) was observed, particularly during high PM periods, implying that nitrate formed in polluted areas interacted with clouds and significantly impacted the regional background site~~ than the evaporative period (3 %). Overall, our ~~study underscores~~ results demonstrate the importance of ~~understanding the dynamics of secondary organic aerosols~~ SOA and the ~~impacts~~ influences of cloud ~~processing~~ processes in regional ~~mountainous~~ mountain areas in southeastern China.

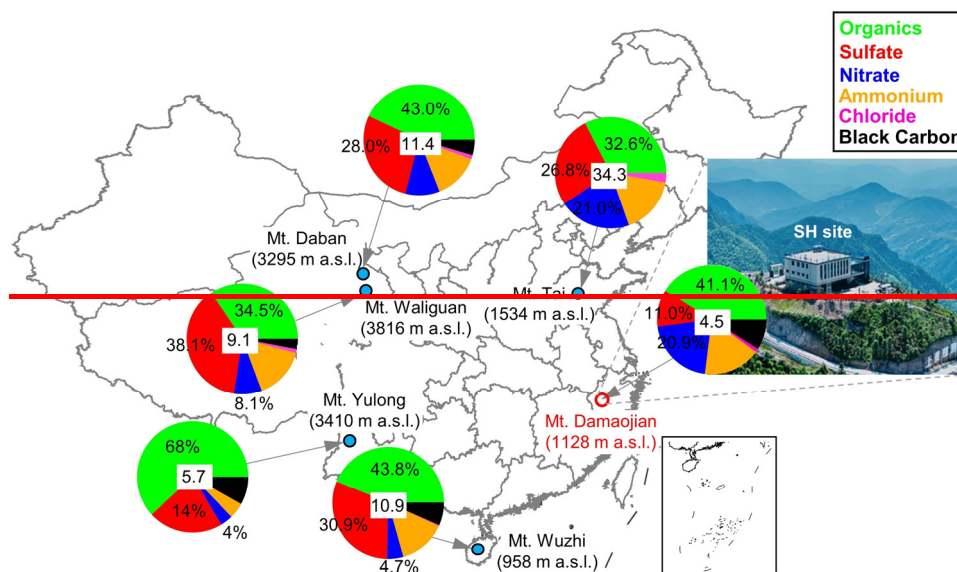
1 Introduction

40 Aerosol particles play essential roles in regional and global climate (Ramanathan et al., 2001; Kanakidou et al., 2005), as well as air pollution (Huang et al., 2014) and public health (Kampa and Castanas, 2008). Submicron aerosol (PM₁) from both natural and anthropogenic sources can be transported to the upper layer level of atmospheric boundary layer or even lower free troposphere through convection and frontal uplift (Monks et al., 2009; Huang et al., 2020; Carbone et al., 2014). At high altitudes, aerosol species can be transported over longer distances, depending on their particle sizes and compositions
45 (Pokorná et al., 2022; Tang et al., 2016; Zhong et al., 2022), and the aging processes during transport results in continuous changes in chemical and physical properties (Calvo et al., 2013; Hallquist et al., 2009). ~~High-altitude aerosols~~ Aerosols can ~~serve as cloud condensation nuclei or ice nuclei~~ have an important impact on CCN properties at high altitudes where atmospheric conditions favour the formation of clouds, thereby affecting the lifetime and optical properties of clouds through aerosol-cloud interactions (Haywood and Boucher, 2000). ~~They can also have potential impacts on ground-level air pollution through downward mixing~~ (Timonen; Asmi et al., ~~2013~~ 2012; Rejano et al., 2021). On the other hand, aerosol-cloud interactions also modify the chemical composition of aerosols within cloud droplets. This modification, in turn, affects the characteristics of surrounding aerosols after the cloud has evaporated (Roth et al., 2016). As a result, measurements of high-altitude regional aerosols are of great importance for a better understanding of aerosol-cloud interactions and their impacts on air pollution and climate.

55 Mountain sites are crucial platforms for studying aerosol characteristics over regional scales scales and the influences of diverse emission sources (e.g., biomass burning, industrial process, and biogenic emissions) and atmospheric processes (e.g., in-cloud processing, new particle formation). Compared to balloon and aircraft observations, mountain sites have advantages in continuous and long-term observations ~~because of low cost, stable geographic location, and accessibility for instrument~~ maintenance. In addition, the different meteorological conditions at mountain sites can have great impacts on aerosol
60 formation ~~aerosol formation~~, aging, and scavenging patterns. For example, Gao et al. (2023) showed that cloud processes can promote the formation of secondary organic aerosol (SOA) by multiphase oxidation. Li et al. (2013) found that high relative humidity (RH) at Mt. Hua can lead to a reduction in particle acidity, and thus reduce the formation of biogenic SOA by suppressing the acid-catalysis reaction. Chen et al. (2021) reported that fog scavenging was more efficient towards particles with aerodynamic diameter larger than 700 nm in Taiwan mountain regions, while smaller particles ~~could continue to grow~~ via remained growth through the process of gas-to-aqueous partition partitioning. Although several ~~studies over mountain~~

~~sites have been conducted to characterize chemical composition and sources several~~ mountain stations have been ~~settled~~established in China to gain more information on the chemical composition and sources (Zhang et al., 2018; Zhang et al., 2019; Du et al., 2015; Zhang et al., 2014), optical properties (Wang et al., 2015), and hygroscopic properties of aerosols (Ding et al., 2021), most of ~~them~~these studies are mainly conducted on Qinghai-Tibetan Plateau and in Northern China Plain (NCP), while the studies in southeastern China ~~is very~~remain limited.

In this work, a high-resolution time-of-flight aerosol mass spectrometer (AMS hereafter) and a quadruple aerosol chemical speciation monitor (ACSM hereafter) were deployed at a forested mountain site in southeastern China. The chemical composition and properties of PM₁ are characterized, the elemental composition and oxidation state of OA are determined, and the potential transport pathways of PM₁ are also investigated using back trajectory analysis. Furthermore, the effect of cloud processes on aerosol species is ~~also~~ discussed. The sources of organic aerosol are investigated using positive matrix factorization (PMF) analysis of combined high-resolution organic and inorganic aerosol mass spectra. Particularly, particulate organic nitrates (ONs) are determined and quantified based on PMF results. Finally, the potential transport pathways of PM₁ are investigated using backward trajectory analysis.



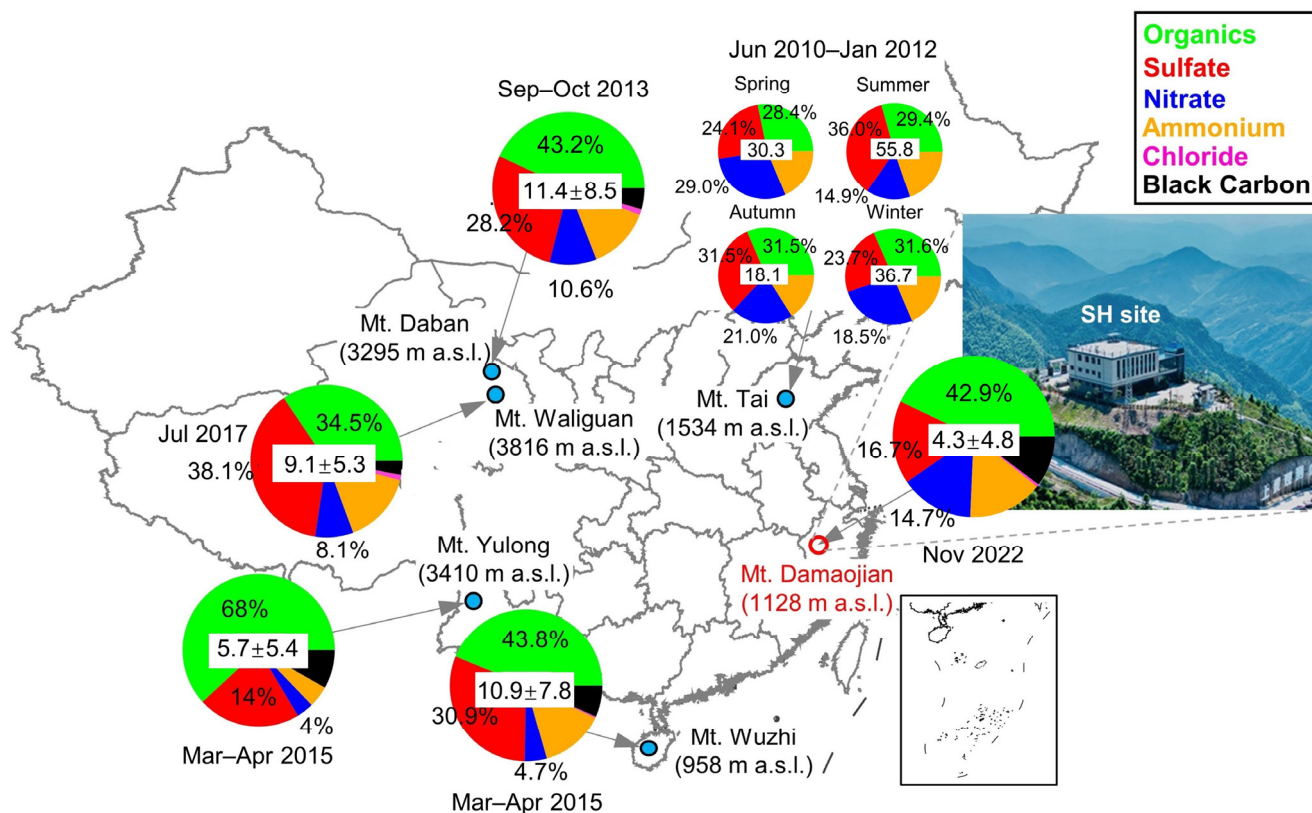


Figure 1. Location of the sampling site- (Mt. Damaojian, red circle on the map). The mean concentration ($\mu\text{g m}^{-3}$) and chemical composition of submicron aerosols (NR-PM₁+ BC if it was available) measured at selected mountain sites in China are also shown. Note that BC and chloride are not accounted for Mt. Tai due to the lack of measurement or data in the relevant study. Detailed information of these sampling sites is presented in Table S1 in the Supplement.

2 Methods

2.1 Site and instrumentation

The campaign was carried out from 1 November to 30 November 2022 at Shanghuang ~~Atmospheric Boundary Layer and Eco-Environment~~ Environmental Observatory of Chinese Academy of Sciences (SH-site on the top of), located at Mt. Damaojian (119.51°E, 28.58°N, 1128 m a.s.l.) in Wuyi County, Zhejiang Province (Fig. 1). This site is a typical background site in southeastern China that is surrounded by mountains and forests, and there are no strong local anthropogenic sources nearby.

PM₁ species were measured using a suite of real-time instruments with 1–520 min time resolution, including an AMS operated under the “V-mode” and a quadrupole ACSM for non-refractory (NR)-PM₁ composition, together with a seven-wavelength Aethalometer (AE33, Magee Scientific Corp.) for equivalent black carbon (BC) mass concentration. The AMS measurements were only conducted during two periods (15–20 November and 24–28 November, respectively) in this study

100 due to the malfunction of the instrument. Briefly, aerosol particles were sampled into an air-conditioned room through stainless steel tube (O.D.: 1/4 inch), and the residence time was estimated as 5 s. -A nafion dryer was placed upstream of the ACSM and AMS to remove the moisture, after that, aerosol particles were sampled into AMS, ACSM, and AE33, respectively. Because there was no size cutoff in front of the sampling line, the AMS and ACSM may report slightly higher concentrations than expected because of measuring some cloud droplets larger than 2.5 μm . According to a previous study during three fog episodes at a rural site in North China Plain, the influence of fog droplets on submicron aerosol measurements was less than 20% (Kuang et al., 2024). Simultaneously, air pollutants including NO_x , O_3 , ~~$\text{PM}_{2.5}$ and PM_{10}~~ were measured by a suite of gas analyzers (Thermo Scientific Inc., USA), $\text{PM}_{2.5}$ and PM_{10} were measured using continuous ambient particulate monitors with $\text{PM}_{2.5}$ and PM_{10} cutoff before the sampling inlet (Model 5014i, Thermo Scientific., USA), and CO was measured by a Picarro greenhouse gas analyzer (G2401, Picarro Inc., USA). ~~In addition, meteorological~~ Meteorological parameters containing temperature (T), **RH**, wind speed (WS), wind direction (WD), and pressure (P) were measured ~~at the same site~~ by an automatic weather station. In addition, (PDR). More details and descriptions of the instruments and data are provided in Table S1.

2.2 Data analysis

2.2.1 ACSM and AMS

115 ACSM data were analyzed using ACSM standard data analysis software (v2.5.13) and AMS data were analyzed using SQUIRREL v1.65F and PIKA v1.25F. A composition-dependent collection efficiency (CDCE) was applied to the ACSM/AMS data according to Middlebrook et al. (2012). Elemental analysis of high-resolution mass spectra (HRMS) was performed using the “Improved-Ambient” (I-A) method (Canagaratna et al., 2015). The default relative ionization efficiency (RIE) values of 1.1, 1.4, and 1.3 were applied for nitrate, organics, and chloride- (Canagaratna et al., 2007; Nault et al., 2023). According to the ion efficiency (IE) calibration results using ammonium sulfate, the RIE values of ammonium and sulfate were 5.05 and 0.73 for ACSM, and 5.26 and 1.28 for AMS, respectively. Detailed comparison of the concentrations of NR- PM_1 species measured by AMS and ACSM are shown in Fig. S1. The ACSM data during the sampling period was corrected by using the regression coefficients between ACSM and AMS. As shown in Fig. S1 (Figs. S1g and h, after this adjustment, the concentrations of NR- PM_1 tracked well with $\text{PM}_{2.5}$ and PM_{10} measured by gas analyzers ($r^2 = 0.7060$ and slope = 0.66, 48 for ACSM, $r^2 = 0.93$ and slope = 0.54 for AMS respectively) and PM_{10} ($r^2 = 0.53$ and slope = 0.27 for ACSM, $r^2 = 0.99$ and slope = 0.39 for AMS respectively) measured by the particle monitor, suggesting that the AMS/ACSM quantification was

125 reasonable.

PMF Evaluation Tool (PET v3.04) was employed to further deconvolve the HRMS derived from AMS into different source factors following the procedures reported by Ulbrich et al. (2009) and Zhang et al. (2011). In addition to organic fragment ions, the major fragment ions of inorganic species, i.e., SO^+ (m/z 48), SO_2^+ (m/z 64), SO_3^+ (m/z 80), HSO_3^+ (m/z 81), H_2SO_4^+

(m/z 98) for sulfate, NO^+ (m/z 30), NO_2^+ (m/z 46) for nitrate, NH^+ (m/z 15), NH_2^+ (m/z 16), NH_3^+ (m/z 17) for ammonium, and Cl^+ (m/z 35), HCl^+ (m/z 36) for chloride were also included into the HR data and error matrices for PMF. A more detailed description of the procedures was given in Sun et al. (2012). After checking the key diagnostic plots (Fig. S2), mass spectra, and the correlations with related tracers, a four-factor solution was considered as the optimal solution in this study- (Text S1).

2.2.2 Estimation of organic nitrates

ONs were estimated from the PMF results (Zhang et al., 2011; Xu et al., 2015). Briefly, NO_x^+ (i.e., NO^+ and NO_2^+) are major fragments of nitrate functionality ($-\text{ONO}_2$), which can be referred to as the total nitrate measured by AMS. Combining inorganic with organic mass spectra in PMF, NO^+ and NO_2^+ can be separated into different organic aerosol (OA) factors and an inorganic nitrate aerosol factor (NIA). According to previous studies, the ratios of $\text{NO}^+/\text{NO}_2^+$ for ONs are approximately 2.25–3.7 times higher than pure NH_4NO_3 (Fry et al., 2013; Fry et al., 2009). Consistently, the PMF results in our study (Fig. 7) show that the average $\text{NO}^+/\text{NO}_2^+$ ratios of LO-OOA and MO-OOA were 13.19 and 11.2, falling within the range of ONs. In contrast, a $\text{NO}^+/\text{NO}_2^+$ ratio of 3.56 was observed for NIA, reflecting its characteristics of inorganic nitrates. Therefore, the mass concentration of ONs ($\text{NO}_{3,\text{org}}$) was calculated by summing these two ion signals distributed in all OA factors as follows:

$$\text{NO}_{3,\text{org}} = \text{NO}_{\text{org}}^+ + \text{NO}_{2,\text{org}}^+ \quad (1)$$

$$\text{NO}_{\text{org}}^+ = \sum([\text{OA factor}]_i \times f_{\text{NO}^+,i}) \quad (2)$$

$$\text{NO}_{2,\text{org}}^+ = \sum([\text{OA factor}]_i \times f_{\text{NO}_2^+,i}) \quad (3)$$

where $[\text{OA factor}]_i$ represents the mass concentration of OA factor i resolved by PMF, $f_{\text{NO}^+,i}$ and $f_{\text{NO}_2^+,i}$ are the mass fractions of NO^+ and NO_2^+ in OA factor i , respectively.

2.2.3. Backward trajectory analysis

The Hybrid Single-Particle Lagrangian Integrated Trajectories (HYSPLIT) model and meteorological data from the NOAA Global Data Assimilation System (GDAS) were used to calculate 72 h backward trajectories at the SH site. The trajectory arrival time was set from 0:00 to 23:00 at 1 h intervals, and the arrival height at the site was set as 1100 m. To further show the aerosol particle concentration levels in different regions, the map was coloured by the time-averaged organic carbon surface mass concentration (ENSEMBLE) from the M2T1NXAER v5.12.4 dataset ($0.5 \times 0.625^\circ$, hourly). This dataset, part of the Modern-Era Retrospective analysis for Research and Applications version 2 (MERRA-2) model, which (Gelaro et al., 2017), was obtained sourced from the NASA Giovanni website (<http://giovanni.sci.gsfc.nasa.gov/giovanni>)-<https://giovanni.gsfc.nasa.gov>).

3. Results and discussion

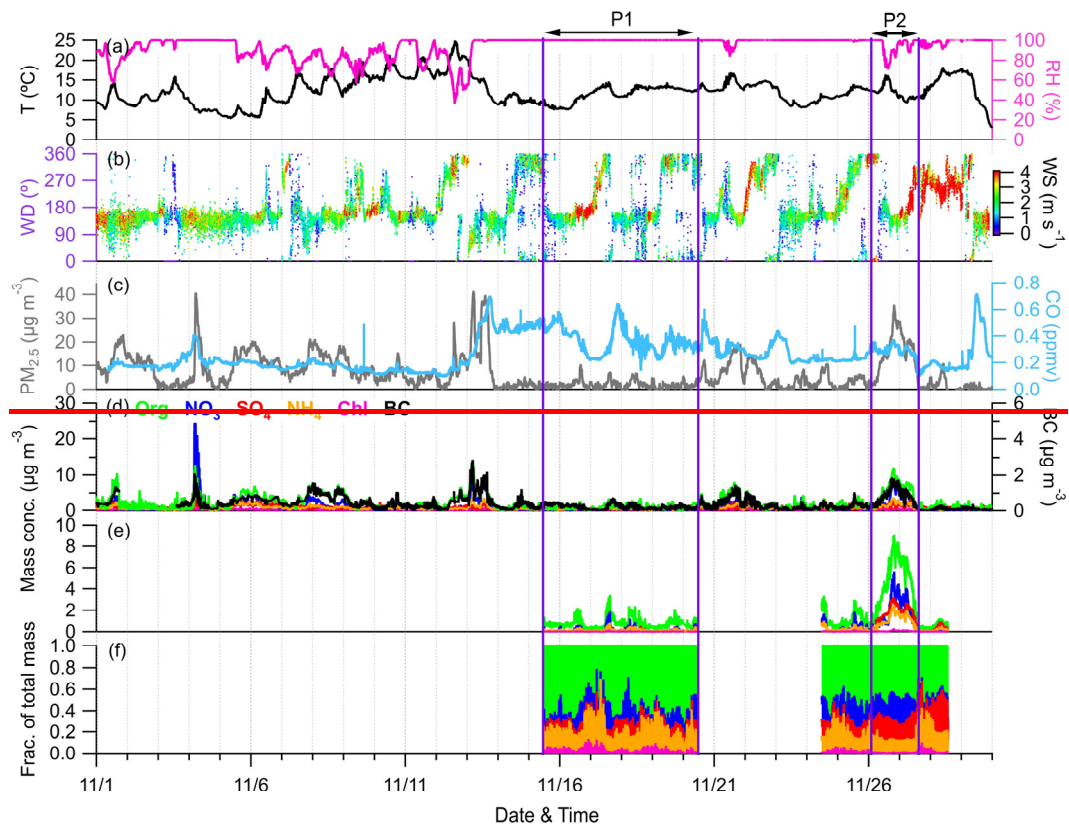
3.1. General descriptions

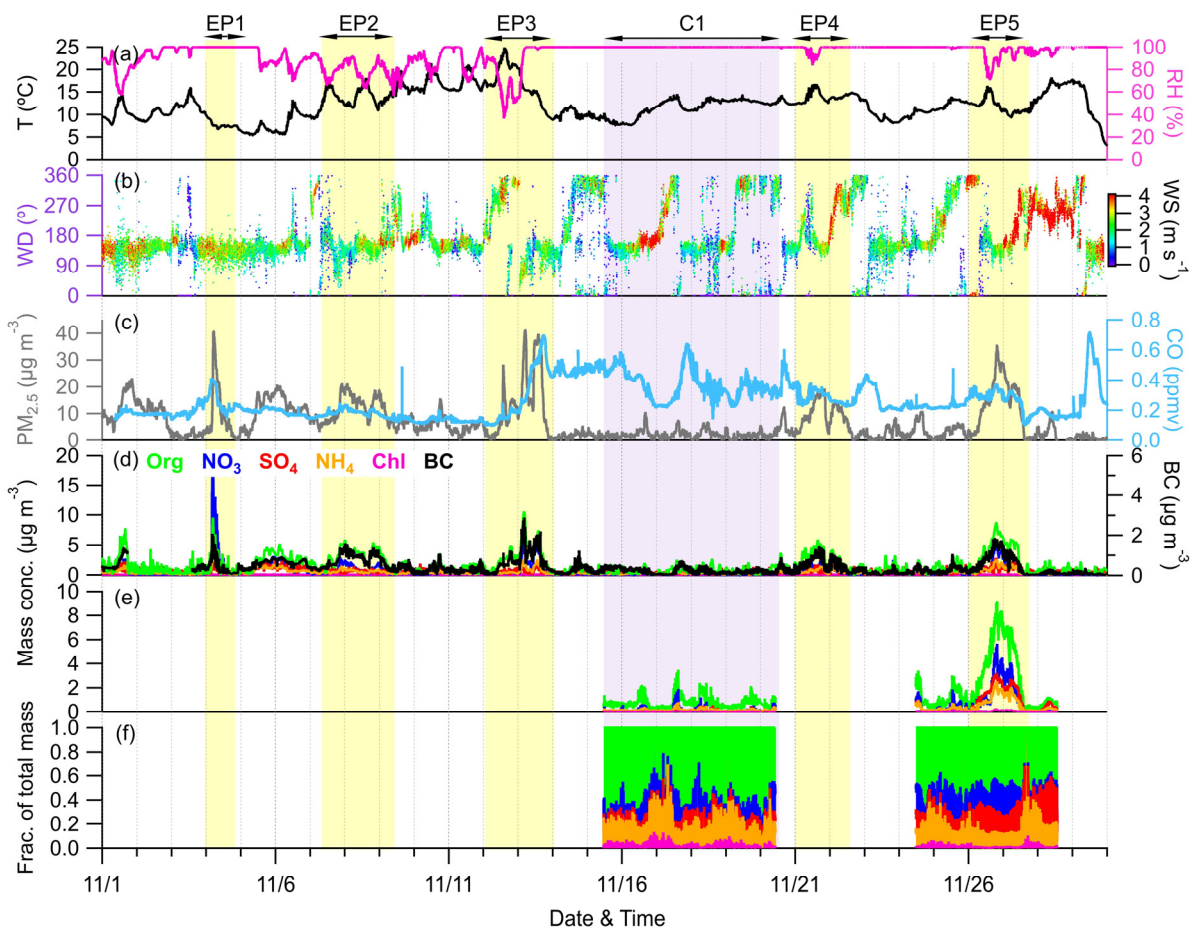
3.1. Mass concentration and chemical composition of submicron aerosols

Figure 2 shows the time series of meteorological parameters (T , RH, WD, and WS), air pollutants ($PM_{2.5}$ and CO) along with PM_1 (NR- PM_1 + BC) species during the campaign. The total PM_1 concentration varied dynamically from $0.3 \mu g m^{-3}$ to $57.9539.8 \mu g m^{-3}$ during the whole sampling period, with an average ($\pm 1\sigma$) of $4.45 \pm 6.513 \pm 4.8 \mu g m^{-3}$. As shown in Fig. 1, organics ~~held~~ accounted for the largest contribution (42.9 %) to the total PM_1 during the sampling period (41.1 %), followed by nitrate (20.9 %), sulfate (16.7 %), ammonium (17.15.0 %), sulfate (11.0) nitrate (14.7 %), BC (9.0) 10.2 %, and chloride (4.0.5 %). In addition, BC was observed to correlate well with PM_1 and $PM_{2.5}$ ($r^2 = 0.59$ and 0.62, respectively), suggesting that the aerosol particles at this site may be largely influenced by the regional biomass burning plumes in the Yangtze River Delta (Zhang et al., 2015). The concentration and composition of PM_1 are quite different from those observed at other Chinese mountain sites with similar altitudes in different seasons (Fig. 4), such as Mt. Wuzhi, where PM_1 has a mean mass concentration of $10.9 \mu g m^{-3}$, and sulfate makes up a significant part (30.9 %) of total PM_1 (Zhu et al., 2016). Note that the 1). For example, the average PM_1 concentration at SH site is even here is much lower compared to Mt. Wuzhi ($10.9 \pm 7.8 \mu g m^{-3}$) at a similar altitude, and is also lower than those at mountain sites with at higher altitude (Fig. 4), altitude mountains such as Mt. Tai (34.3) Yulong ($5.7 \pm 5.4 \mu g m^{-3}$) in NCP (Zhang et al., 2014), and Mt. Yulong ($5.4 \mu g m^{-3}$) (Zheng et al., 2017), and Mt. Waliguan ($9.1 \pm 5.3 \mu g m^{-3}$). Although PM_1 concentration has a strong seasonal dependence, such as in Mt. Tai, with low concentration in autumn ($18.1 \mu g m^{-3}$) (Zhang et al., 2019), and high in summer ($33.5 \mu g m^{-3}$), the average PM_1 concentration at our site is still much lower than Mt. Daban ($11.4 \mu g m^{-3}$) and Mt. Tai in the same season (autumn, 2019). Considering the occurrence of frequent cloud events during the sampling period, the low PM_1 concentration might be mainly associated with cloud scavenging (Kim, which will be further validated in subsequent sections. Notably, a relatively lower contribution of sulfate to PM_1 was observed (16.7 %) in this site compared to other mountain sites (14.0 %–38.1 %), which was likely attributed to the significant reduction of SO_2 emission in China during the past decade (Wen et al., 2023). The decrease in sulfate contribution was associated with an elevation (et al., 2019). Indeed, the unexpectedly high fraction of nitrate at the regional background site might indicate contribution. This shift suggests that most NH_4 will probably be in the form of ammonium nitrate formed from which is more volatile than ammonium sulfate and thus unlikely to transport over a large scale. Notably, at Mt. Tai, even though the contributions of sulfate were high, nitrate still accounted for considerable fractions (14.9 %–29.0 %) that were comparable to this site (20.9 %). Taken together, PM_1 at this site is more likely influenced by anthropogenic-emitted NO_x can have a significant impact on emissions over a smaller regional scale in the southeastern China. One explanation was that nitrate formed in polluted regions interacted with clouds and affected the regional nitrate level as cloud evaporates (Tao et al., 2018), consistent with the high urban density in eastern China.

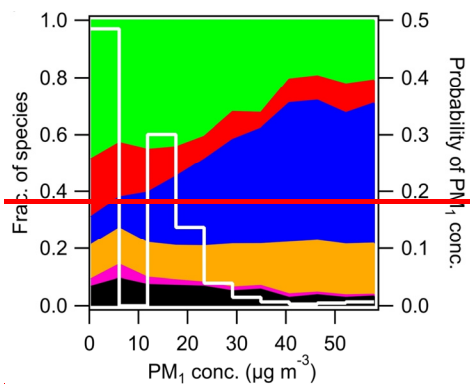
Figure 33a shows the relative contribution of each PM_1 component as a function of PM_1 concentration together with the probability density of PM_1 mass loading. The highest two probabilities frequencies of PM_1 concentrations were distributed

within 0–63 $\mu\text{g m}^{-3}$ and 12–185–8 $\mu\text{g m}^{-3}$ (48.529.0 % and 30.129.8 %, respectively). The fraction of nitrate increased significantly with PM_{10} concentration, and meanwhile, the fraction of organics and BC exhibited a decreasing trend. ~~This result suggested that high levels of PM_{10} at the SH site might be mainly attributed to the nitrate formation and transport. It is also~~We noted that a nitrate-dominant peak of PM_{10} mass loading was observed at the nighttime of 4 November (Fig. 2d), which was associated with the corresponding increase in CO_2 , further emphasizing the contribution of transport to nitrate (Fig. 2d), and the concentrations of organic and nitrate as a function of PM_{10} mass during this event and the rest of the campaign are shown in Fig. S3. Almost all the data points with PM_{10} concentrations above 20 $\mu\text{g m}^{-3}$ were from this event. During EPI, a steeper slope for nitrate relative to PM_{10} was found than that for organics, which was contrary to slopes during the rest period (Fig. S3). These distinct differences in slopes for nitrate and organics implied different mechanisms of PM_{10} elevation during these two periods. Consequently, we also excluded EPI from the statistic of Fig. 3a, and the result is presented in Fig. 3b. After removing EPI, organics became the dominant contributor (> 40 %) across all PM_{10} concentrations. Despite this, there was still an increasing trend for nitrate and a decreasing trend for sulfate along with increased PM_{10} , yet the contribution of ammonium remained relatively constant. This further supported our previous hypothesis that there was a conversion of ammonium sulfate to ammonium nitrate with the increase in PM_{10} concentration. Overall, these results suggested that high levels of PM_{10} at the SH site might be mainly attributed to the formation or transport of organics, meanwhile, nitrate also plays a nonnegligible role.





210 **Figure 2.** Time series of (a) T and RH; (b) WD coloured by WS; (c) mass concentration of $PM_{2.5}$ and mixing ratio of CO; (d) mass concentrations of NR- PM_1 species measured by ACSM together with BC measured by AE33; and (e, f) mass concentrations and contributions of NR- PM_1 species measured by AMS. The yellow and purple shaded areas represent six selected episodes (EP1–EP5 and C1, respectively).



215

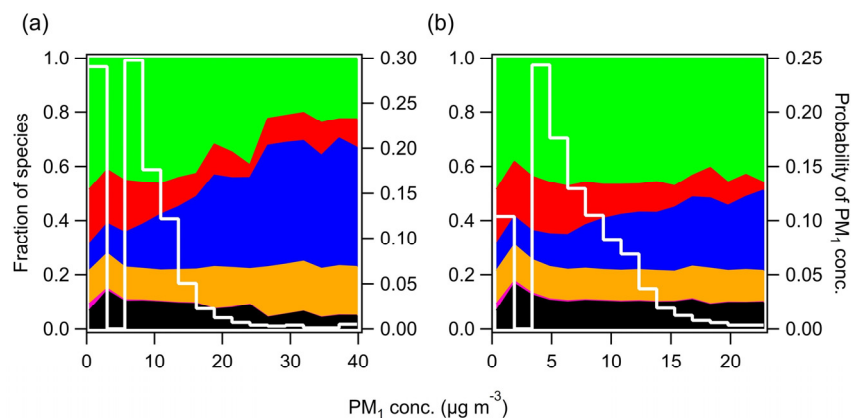


Figure 3. Variations of aerosol composition as a function of PM₁ mass concentration and the probability density of PM₁ during (a) the entire campaign study period and (b) the period excluding EP1.

220 The diurnal cycles of PM₁ species, air pollutants, and meteorological parameters during the entire campaign are illustrated in Fig. S3. The mean and median values of organics and nitrate both showed distinct noon peaks at around 14:00, which could be attributed to the daytime photochemical production and the low wind speed (Tang et al., 2022; Xu et al., 2018b). In addition, these noon peaks may also be related to the development of atmospheric boundary layer, which facilitates the mixing of air masses transported from polluted areas. The high nighttime peak of nitrate was mainly due to the influences of

225 the nitrate event on 4 November. Comparatively, sulfate, chloride, and BC showed relatively flat diurnal variations, suggesting the regional characteristics of these species (Zhang et al., 2015).

3.2 Comparisons of two different periods

RH plays a crucial role in determining the composition, formation, and evolution of PM_{10} (Sun et al., 2013; Xu et al., 2019). Figure S4 shows the variation of organics, nitrate, and sulfate mass concentrations as a function of RH during the entire campaign. Overall, the mass concentrations of organics decreased significantly with increasing RH, while nitrate and sulfate only showed slight decreases. Previous studies have shown that aerosol mass generally increases on foggy days (Chen et al., 2021). This phenomenon could be due to the cloud scavenging effect under high RH at this site. Another explanation is that submicron aerosols grow to larger sizes under high RH that AMS aerodynamic lens cannot transmit (Chakraborty et al., 2016). To further investigate aerosol characteristics under different meteorological conditions, we selected two periods (Fig. 2, denoted as P1 and P2 hereafter) with largely different humidity and PM_{10} concentrations. P1 was a typical cloud scavenging period with relative humidity remaining to be saturated (RH = 100 %), and meanwhile, PM_{10} stayed at a very low level, with an average value of $1.34 \mu\text{g m}^{-3}$. Whereas in P2, the mean RH decreased to 93.9 % with almost no cloud event, and a high PM_{10} event happened with a maximum mass concentration of $20.65 \mu\text{g m}^{-3}$ (on average $9.39 \mu\text{g m}^{-3}$). Then, the PM_{10} concentration decreased rapidly due to the enhanced mountain-valley wind ($WS > 4 \text{ m s}^{-1}$) and increasing RH (71 % to 100 %) during the nighttime. Therefore, P2 was more likely to be a cloud evaporation period, where aerosol particles were released from the cloud droplets after water evaporation (Fanourgakis et al., 2019), and air mass origin

The entire study period was characterized by five PM_{10} episodes (EP1–EP5), as marked in Fig. 2. Meanwhile, a clean period (C1) with low PM_{10} levels was also selected for comparison. The relationship between the PM_{10} species concentration,

meteorology, and air mass transport during these six periods is shown in Fig. 4 and Fig. S5. EP1 exhibited a nitrate-dominant PM_{10} peak, with nitrate concentration rapidly increased by $\sim 18 \mu\text{g m}^{-3}$ within an hour. In addition, a CO peak was also observed at that time, suggesting potential contributions of pollution transport to nitrate. Given the lack of anthropogenic activities near the sampling site, the enhanced nitrate concentrations likely originated from NO_x transported from adjacent towns in the northeast, as indicated by the nitrate wind polar plot (Fig. S6) showing high levels of nitrate mainly associated with northeastern wind directions. This was further supported by the back trajectory analysis, in which air masses on 4 Nov were also from the northeast. Moreover, the RH was stable at 100% during EP1, which could facilitate the heterogeneous uptake of N_2O_5 and subsequent nitrate formation in the aqueous phase at night (Brown et al., 2006; Li et al., 2020).

In contrast to EP1, PM_{10} in other episodes (EP2–5) were all dominated by organics. EP2 was associated with low concentrations of CO, indicating relatively slight pollution transport influence. In addition, clear and similar diurnal variation patterns were found in aerosol species and RH, suggesting that PM_{10} in this period was mainly affected by the evolution of the atmospheric boundary layer. EP3 was initiated by an organic-only increase under high temperature ($\sim 15\text{--}25 \text{ }^\circ\text{C}$) and low RH ($\sim 40\text{--}80\%$), while other aerosol species remained at very low levels. Considering the low CO levels in this period, the increasing trend of OA could be attributed to the local biogenic emissions. The concentrations of organic, together with other PM_{10} species and CO, were further elevated after air mass sources shifted from southwest to northwest on 13 Nov, which may bring a large amount of aerosols from megacities such as Zhengzhou and Hangzhou to the SH site (Fig. S5c). EP4 and EP5 were two similar episodes, where PM_{10} concentrations were generally associated with the changes in RH and WD. During these two periods, air masses both originated from the west and southwest, but the trajectory distances during EP5 were shorter, suggesting that the air masses transported more slowly in EP5.

Overall, although these episodes had different mechanisms of PM_{10} variation, they were mostly influenced by the transport of western and southwestern air masses, indicating a substantial impact of anthropogenic emissions from big cities like Nanchang and Fuzhou. These areas are marked by higher pollution according to the organic carbon distribution in Fig. S5. However, we have also identified similar transport pathways and even higher CO concentrations during C1 (0.37 ppm on average) than EP2–5 (0.18–0.31 ppm on average), while the PM_{10} concentration stayed at very low levels for the whole period. It is worth noting that PM_{10} peaks in EP2–EP5 all occurred along with RH below 100 %. When the RH returned to 100 %, PM_{10} concentrations gradually diminished to levels comparable to those observed during the clean period (C1). Furthermore, as shown in Fig. S7, there were notable reductions in the mean and median mass concentrations of all PM_{10} species over the entire campaign, ranging between -2.6 %–44.4 % and 2.8 %–50.1 % when RH reached 100 % from conditions of lower RH, respectively. Considering the frequently occurring cloud events at this site, it was most likely that these variations of RH were affected by the cloud process, which may further play an important role in PM_{10} concentrations. Figure S8 shows the particle depolarization ratio measured by the particle lidar during EP5 and C1. During EP5, clouds were identified at ~1 km above the sampling site from 2:00 to 12:00 on 26 Nov (Fig. S8a). As expected, these clouds gradually disappeared afterward, possibly owing to strong solar radiation at noon on the mountaintop causing cloud droplet evaporation. Meanwhile, a large amount of aerosol particles ($PDR = \sim 0.15$) was released from the clouds, which exhibited a strong agreement with the timing of the PM_{10} peak. These particles were then scavenged by the increased RH and strong wind ($WS > 4 \text{ m s}^{-1}$). This cloud evaporation phenomenon was also found in urban Guangzhou, which caused remarkably enhanced nitrate mass concentration at noon (Tao et al., 2018). In contrast, no such evaporation process was observed during C1 (Fig. S8b). Instead, high PDR values were found generally at around 0 km, which means that clouds constantly existed near the sampling area during this period, coinciding with the constant 100% RH. Therefore, PM_{10} transported to this site was likely to be scavenged by the cloud during C1. These findings were also evidenced by the photos taken at this site at local time ~15:00 on 19 Nov and 26 Nov, where severe cloud cover was observed in C1 (Fig. S9a), yet the weather was generally sunny and cloudless in EP5 (Fig. S9b). As a result, besides regional transport, cloud processes can also have significant impacts on aerosol particles at this site.

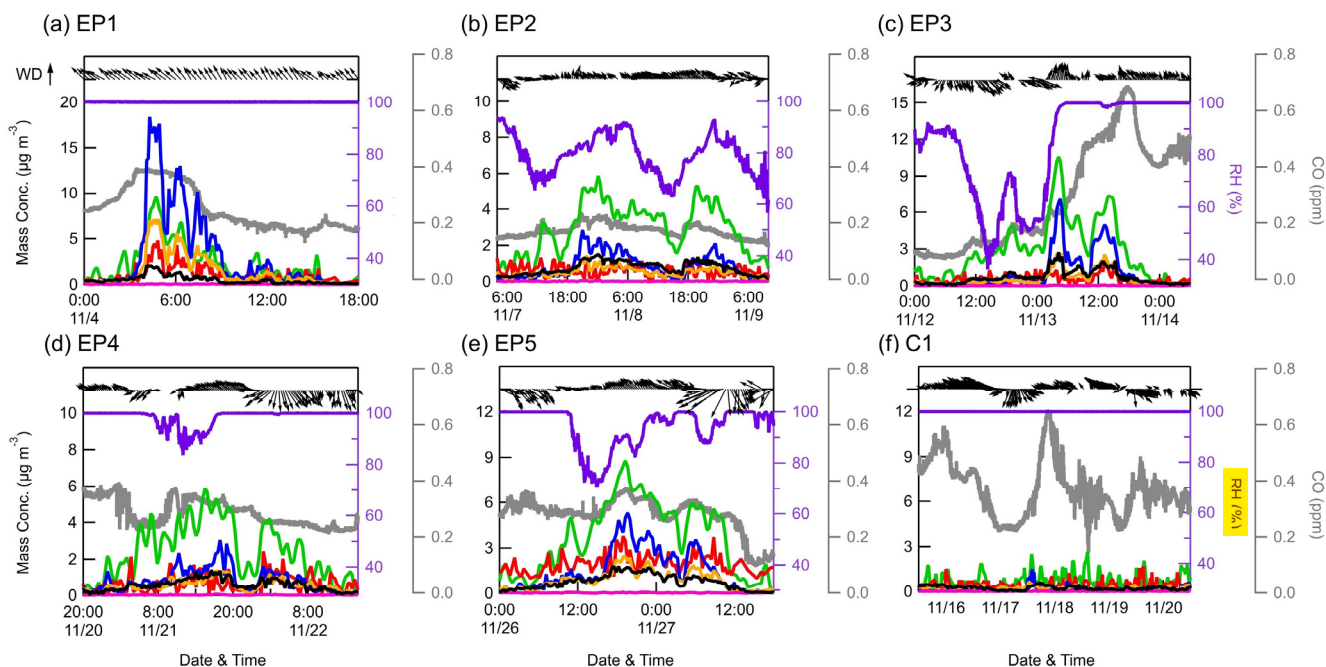


Figure 4. Temporal variations of NR-PM₁ species measured by ACSM, as well as CO, RH, WD, and WS during six case events.

3.3 Impacts of cloud processes on submicron aerosols

To further explore the impacts of cloud scavenging and cloud evaporation on aerosol characteristics, we select C1 and EP5, in which NR-PM₁ were also measured by AMS, for further investigation in this section.

3.3.1 Size distributions and composition

The average chemically resolved size distributions of NR-PM₁ during P4C1 and P2EP5 are shown in Fig. 45. Generally, all species were distributed in accumulation mode in both periods. However, a smaller peak size (300–500 nm) and broader size distribution were observed during P4C1 when compared to those of P2EP5 (~700 nm), probably owing to the wet removal of larger and hygroscopic particles in P4C1 (Ge et al., 2012). Ammonium Also, the complex and broad size distribution observed in C1 suggests that these smaller particles are likely externally mixed with organics, which may further imply the potential formation of SOA from local biogenic sources. In contrast, the uniform size distribution across all particulate species in EP5 indicates their well-mixed and highly aged characteristics. Moreover, ammonium showed similar size distribution with sulfate and nitrate during P2EP5, while in P4C1, it was mixed mainly with sulfate and exhibited a quite different size distribution with nitrate, indicating the potential contribution of organic nitrate.

Clear differences were also found in aerosol composition during P4C1 and P2EP5. Organics were the dominant contributor to total NR-PM₁ mass during P4C1 (68 %), followed by nitrate (12 %), ammonium (11 %), and sulfate (8 %). In contrast,

despite the decreased contribution of organics (51 %), the mass fractions of sulfate and nitrate increased considerably during **P2** (**P17-EP5** (by 9.4% and +9-7.0%, respectively). These changes in the mass fraction of species were attributed to the lower mass scavenging efficiency of organics than inorganic species (Gilardoni et al., 2014). The average HRMS of OA during **P4C1** and **P2EP5** are presented in Fig. **S5S10**. The HRMS of OA were quite similar for the two periods, with a significant peak m/z 44 (mainly CO_2^+). The OA was highly oxidized, with $\text{C}_x\text{H}_y\text{O}_1^+$ dominating the total OA in **P4C1** and **P2EP5** by 41 % and 40 %, followed by C_xH_y^+ (31 % and 32 %), and $\text{C}_x\text{H}_y\text{O}_2^+$ (20 % and 19 %). The contributions of the two major oxygen-containing ion fragments ($\text{C}_x\text{H}_y\text{O}_1^+$ and $\text{C}_x\text{H}_y\text{O}_2^+$) at the SH site were much higher than those at various urban or suburban sites in China, such as 37.4 % in urban Nanjing (Wang et al., 2016), and 52.9 % in suburban Lanzhou (Tang et al., 2022). Note that higher fraction of CO_2^+ (3 % higher) was found in **P4C1** than **P2EP5** (Fig. **S5eS10c**), indicating a higher oxidation degree of OA in **P4C1** (Xu et al., 2014). This is consistent with the higher O/C and OSc in **C1** (0.96 and 0.49) in **P1** than **P2EP5** (0.85 and 0.21).

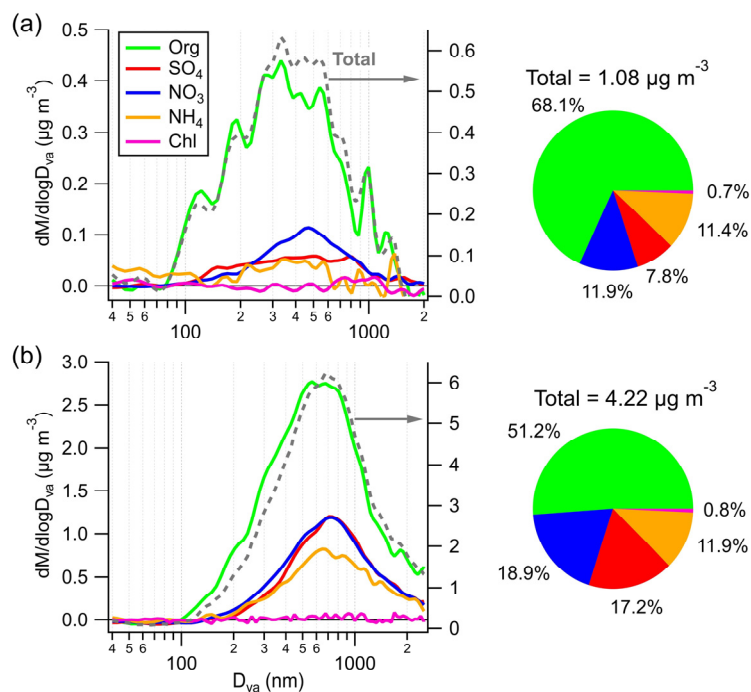
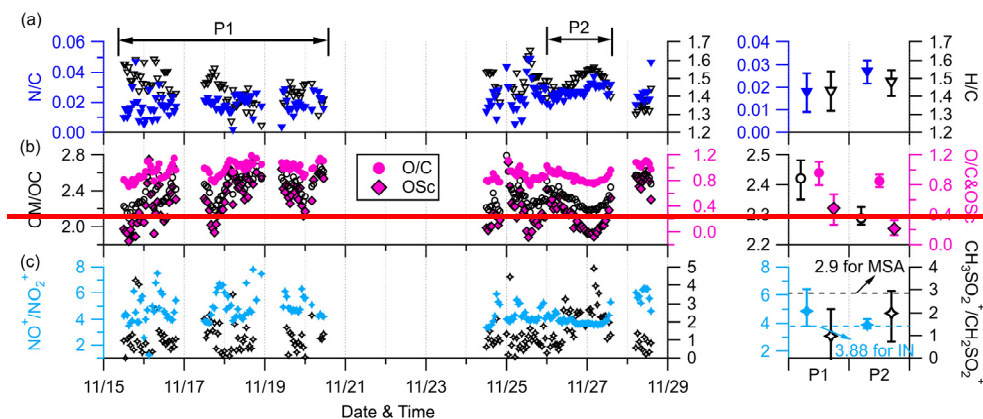


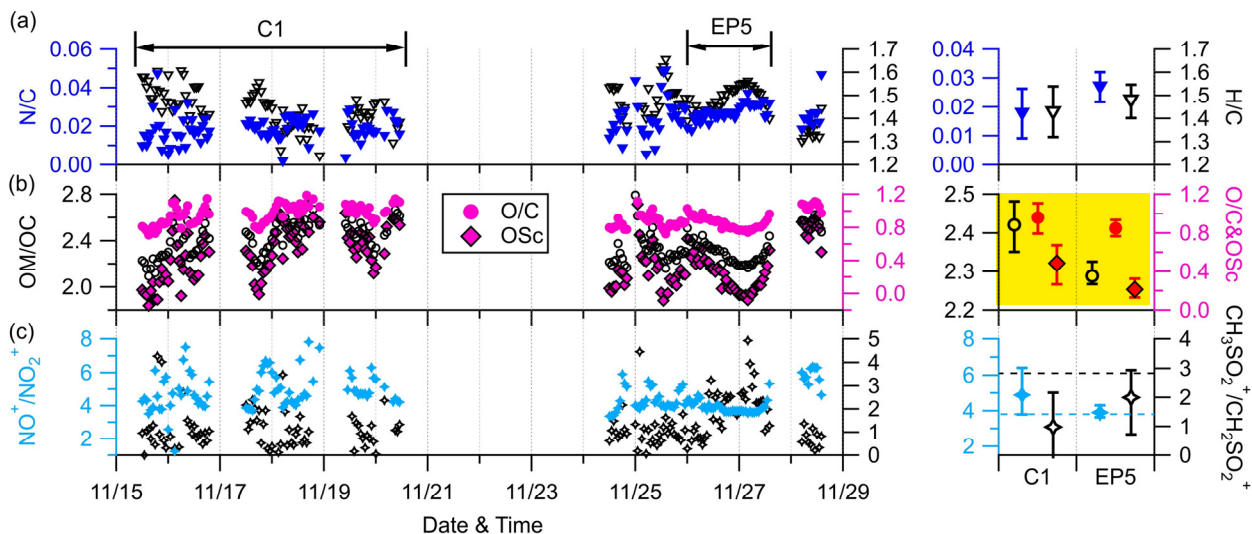
Figure 45. Averaged size distributions and chemical composition of NR-PM₁ during (a) **P4C1** and (b) **P2EP5**.

320

3.3.2.2 Elemental ratios

Figure 56 shows the time series and box plots of N/C, H/C, OM/OC, O/C, and carbon oxidation state (OSc) of OA, as well as two ion ratios at the SH site. The hourly averaged ratios were only reported for periods with OA concentrations above $0.7 \mu\text{g m}^{-3}$. The average N/C ratios were 0.018 for P1 and 0.027 for P2, consistent with the higher fraction of $\text{C}_x\text{H}_y\text{N}_p^+$ in OA during P2. OA had a slightly lower H/C ratio (1.44 vs. 1.48) and higher average ratios of O/C (0.96 vs. 0.85), OM/OC (2.42 vs. 2.29), and OSc (0.49 vs. 0.21) during P1 than those during P2, indicating more oxidized OA during P1. The O/C ratios were overall within the range of 0.94 ± 0.18 at regional background sites (Zhou et al., 2020), yet much higher than those observed at urban and suburban sites. These results suggest that OA at the SH site was relatively well-aged. The ratio of fragment ions NO^+ (m/z 30) to NO_2^+ (m/z 46) is a good indicator for identifying the presence of ONs (Farmer et al., 2010; Lin et al., 2021). The mean ratio of $\text{NO}^+/\text{NO}_2^+$ in P1 was 4.9, which exceeds the value of 3.88 for pure ammonium nitrate (NH_4NO_3 -AN) obtained from the AMS IE calibration, indicating a potential contribution of ONs. Conversely, the mean $\text{NO}^+/\text{NO}_2^+$ in P2 (3.9) was almost identical to that of ANNH_4NO_3 , implying the dominance of inorganic nitrates (INs). Additionally, the CH_2SO_2^+ (m/z 79) and CH_3SO_2^+ (m/z 80) ions were used as signature fragments of methanesulfonate, a typical organic sulfur species generated in marine and remote coastal regions (Chen et al., 2019). However, the mean ratios of CH_3SO_2^+ and CH_2SO_2^+ during P1 and P2 (0.98 and 1.99, respectively) were lower than the value of 2.9 reported in previous studies for MSA, indicating the minimal contribution of MSA (Song et al., 2019). The low contributions of MSA further suggest that aerosols over this region are likely to have negligible oceanic influences. This is also consistent with the back trajectory results in section 3.2, which demonstrate that PM_{10} levels at this site are dominantly influenced by continental sources in the west and southwest.





345 **Figure 56.** Time series and box-plots of 1-hour averaged (a) N/C and H/C, (b) OM/OC, OSc, and O/C, and (c) $\text{NO}^+/\text{NO}_2^+$ and $\text{CH}_3\text{SO}_2^+/\text{CH}_2\text{SO}_2^+$ during the AMS sampling site (left) and their mean values in C1 and EP5 (right). Only ratios determined with good S/N (i.e., organics $> 0.7 \mu\text{g m}^{-3}$) are shown.

The horizontal black and blue dash line in the bottom right plot represent the $\text{CH}_3\text{SO}_2^+/\text{CH}_2\text{SO}_2^+$ value for pure MSA (2.9) and the $\text{NO}^+/\text{NO}_2^+$ value for pure NH_4NO_3 (3.88), respectively.

350 3.4 Source apportionment of OA and contribution of organic nitrates

Four factors were resolved by PMF, including three types of SOA and one inorganic factor: less oxidized oxygenated OA (LO-OOA), more oxidized oxygenated OA (MO-OOA), OA associated with sulfate ions (SO_4 -OA), and inorganic nitrate aerosol (NIA). These four factors together on average accounted for 87.5 % of the total NR- PM_{10} mass. The mass spectra profiles and OA ion family composition of the four factors are shown in Figs. 67 and 78.

355

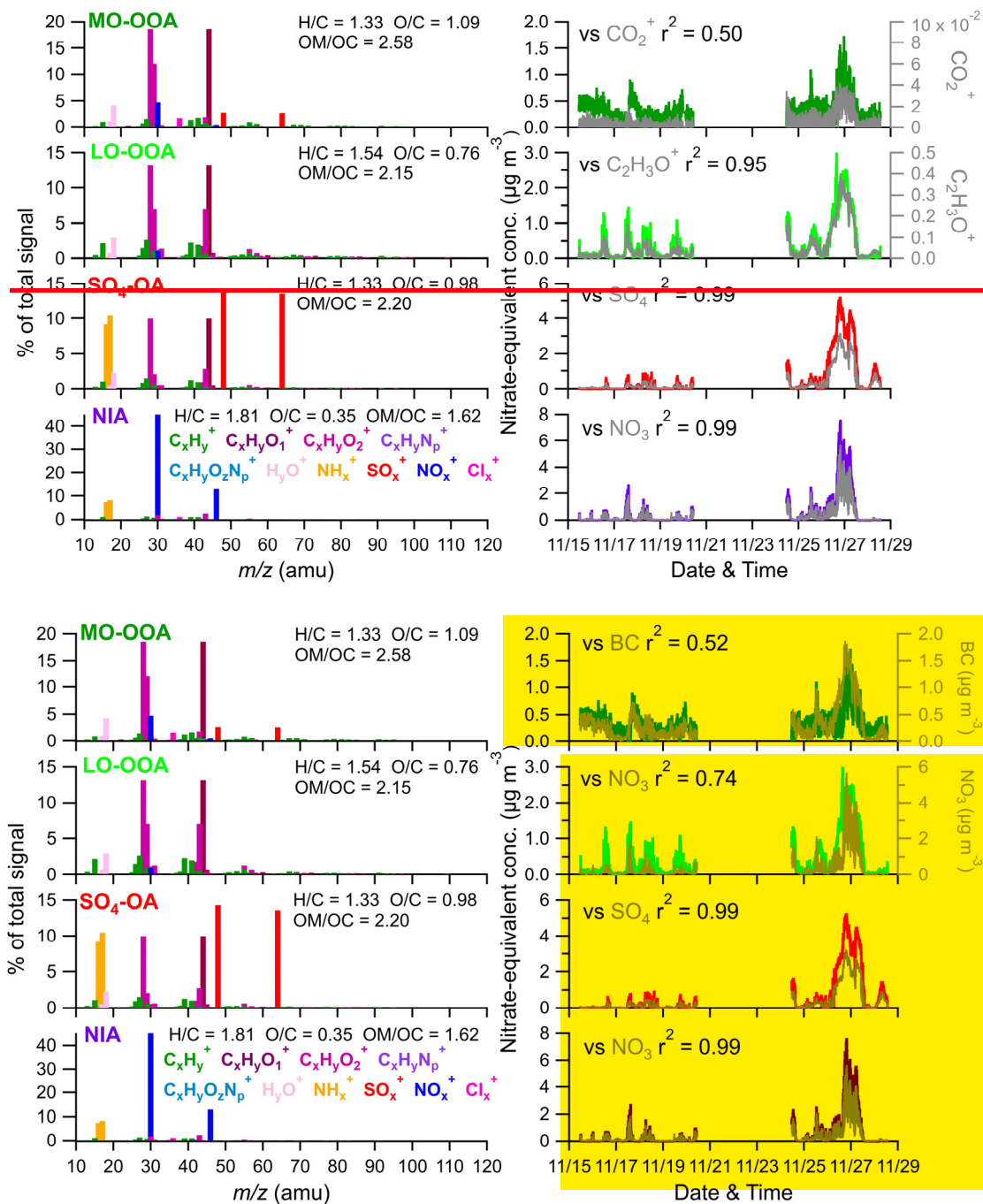


Figure 67. High-resolution mass spectral profiles (left) and time series (right) of four factors. The correlations of four factors with corresponding tracers are also shown.

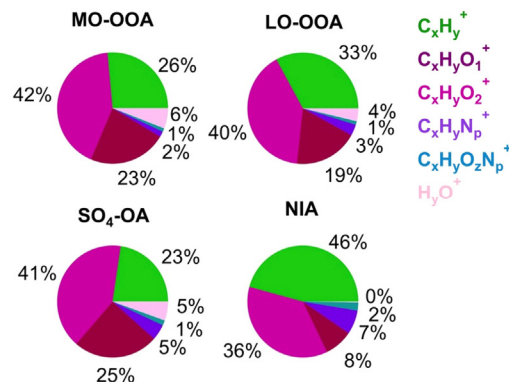
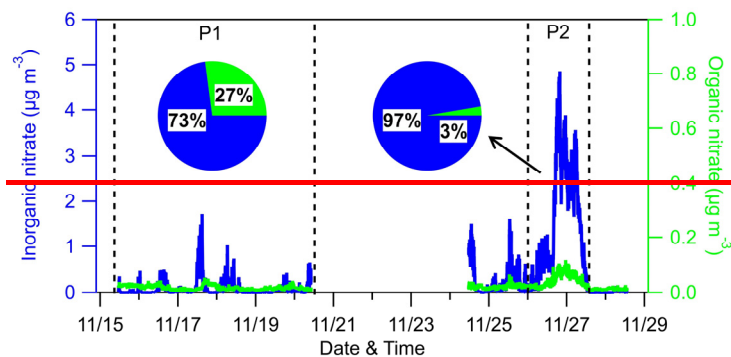


Figure 78. Mass fractional composition of OA ion families for the resolved four PMF factors.

LO-OOA and MO-OOA were identified by prominent peaks of CO^+ and CO_2^+ in the mass spectra. LO-OOA had a high fraction of $\text{C}_2\text{H}_3\text{O}^+$ (m/z 43, 6.8 % of the total signal), while MO-OOA, corresponding to more oxidized and aged components, had a higher abundance of CO_2^+ (17.6 % vs. 12.8 %), $\text{C}_x\text{H}_y\text{O}_2^+$ (23 % vs. 19 %), and O/C ratio (1.09 vs. 0.76) than LO-OOA. The average O/C ratios of these two OOA factors are similar to those at Mt. Bachelor [Observatory](#), where the O/C ratios of SV-OOA and LV-OOA were 0.67 and 1.17, respectively (Zhou et al., 2019). LO-OOA ~~correlated~~ [tightly correlate well](#) with $\text{C}_2\text{H}_3\text{O}^+\text{NO}_3^-$ ($r^2 = 0.95$), ~~and 74~~, [coinciding with their secondary nature. Meanwhile, MO-OOA showed exhibit](#) a moderate correlation with [sulfate BC](#) ($r^2 = 0.56$)-52), [indicating that they were likely coated on BC particles and underwent extensive aging processes during long-range transport.](#) Overall, the LO-OOA and MO-OOA components account for 39.1 % and 29.4 % of the total measured OA mass, respectively (Fig. [S6S11](#)). The mass spectra of the SO_4 -OA factor had a large amount of NH_x^+ and SO_x^+ , together accounting for 48.5 % of the total mass of this factor. Meanwhile, organic components also made up a considerable fraction, yet on average contributing 51 %. It is also noticed that the O/C ratio of the organic fraction of this factor is 0.98, which is even higher than LO-OOA and comparable to MO-OOA, [suggesting that this factor has experienced aging processes during the regional transport. Not surprise As expected,](#) no primary OA factor (e.g., hydrocarbon-like OA, biomass burning OA, etc.) was resolved during this study due to the negligible influences of local emissions, which was consistent with the PMF results at other background sites (Zhou et al., 2019; Zhu et al., 2016).

~~A~~ [An inorganic](#) nitrate aerosol factor was also separated from these OA factors, with nitrates in this factor accounting for 92.6 % of the total NO_x^+ ions. ~~Despite~~ [Apart from](#) NIA, NO_x^+ ions were more assigned in MO-OOA (6.0 % of the total NO_x^+) than LO-OOA (1.4 % of the total NO_x^+), suggesting that ONs were more associated with MO-OOA. [This is contrary to other studies which reported that ONs were more correlated with less oxidized OA \(Zhang et al., 2016; Yu et al., 2019\). According to](#) [One possible reason is that ONs formed and mixed with MO-OOA components during the aqueous aging processes of MO-OOA-coated BC particles. This hypothesis is supported by Cao et al. \(2022\), which demonstrated that ONs exhibit](#)

385 similar volatility to that of MO-OOA when coated on BC. ~~previous studies, the ratios of $\text{NO}^+/\text{NO}_2^+$ for ONs are~~
~~approximately 2.25–3.7 times higher than pure NH_4NO_3 (Fry et al., 2013; Fry et al., 2009).~~ **Consistently,** the average
 $\text{NO}^+/\text{NO}_2^+$ ratios of LO-OOA and MO-OOA were 13.19 and 11.2, falling within the range of ONs. In contrast, a $\text{NO}^+/\text{NO}_2^+$
ratio of 3.56 was observed for NIA, reflecting its characteristics of inorganic nitrates. Based on the PMF results above, the
mass concentrations of ONs during the AMS sampling period were estimated (Fig. 409). Considering ONs as part of
390 organics, we chose a RIE value of 1.4 for the estimated ONs, while a nitrate RIE value (1.1) was correspondingly applied for
INs. ~~The results showed that ONs made a greater contribution to total nitrate in P1 than in P2 (27 % vs. 3 %).~~ This was
~~further supported by the result of Huang et al. (2021), which found that organic nitrate can increase rapidly when $\text{RH} > 70\%$.~~
The average mass concentration of ONs in P1C1 was $30 \pm 22 \text{ ng m}^{-3}$, which was ~~comparable to lower than~~ that in P2EP5 (40
 $\pm 23 \text{ ng m}^{-3}$), ~~likely owing to which can also be explained by the evaporative release of ONs in EP5.~~ However, considering
395 the ~~cloud scavenging slightly elevated values (10 ng m^{-3}) between these two periods, we cannot rule out the possible~~
~~formation of ON from aqueous phase processes (Xian et al., 2023) and gas phase reaction initiated by NO_3 during nighttime~~
~~(Ayres et al., 2015).~~ Also, the low levels of ON might cause uncertainties in its estimation. Since ONs at this site ~~was~~
close to the value (40 ng m^{-3}) ~~obtained reported by Hao et al. (2014) at a forest-urban mixed site in Finland (Hao et al., 2014),~~
~~we considered our quantification of ONs reasonable.~~ However, significant ~~discrepancies differences~~ were observed between
400 the INs mass concentrations during P1C1 and P2EP5 ($0.08 \mu\text{g m}^{-3}$ vs. $1.147 \mu\text{g m}^{-3}$), ~~revealing that).~~ This could be attributed to
~~that water-soluble HNO_3 or NH_4NO_3 was scavenged by cloud droplets and removed by precipitation before transporting to~~
~~this site during C1, while in EP5, these~~ INs dominated the elevation of total nitrate during cloud evaporation ~~in P2.~~ These
~~differences in INs also led to a greater contribution of ONs to total nitrate in C1 than in EP5 (27 % vs. 3 %).~~



405

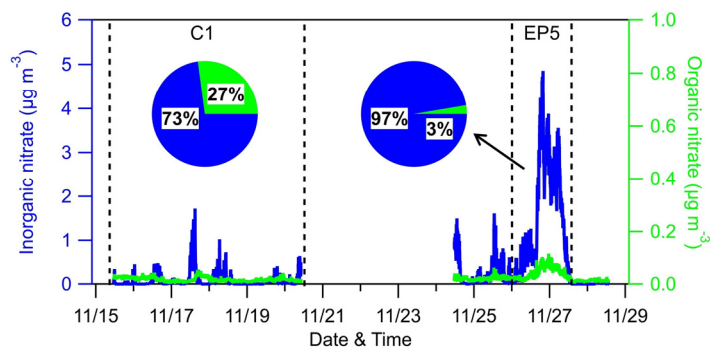
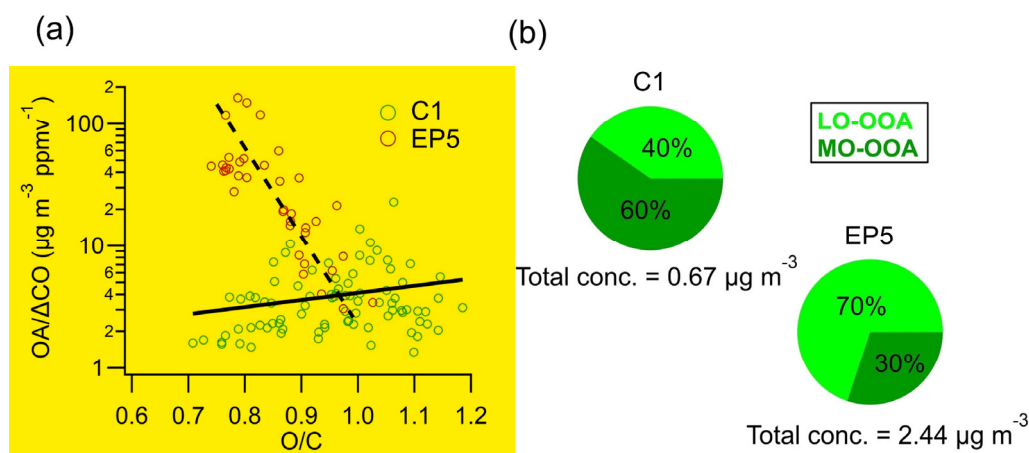


Figure 89. Time series and relative contributions of inorganic nitrate and organic nitrate during the AMS sampling period.



410 **Figure 10.** (a) Scatter plot of OA/ΔCO as a function of O/C ratios and (b) mass concentrations and proportions of MO-OOA and LO-OOA during C1 and EP5.

3.45 Evolution of OA

The formation and evolution of OA can be investigated using the ratio of OA to ΔCO (CO minus background CO) to remove the atmospheric dilution effects (SunDecarlo et al., 2011-2010). In this study, 0.12 ppmvppm (average of the lowest 5 % concentration) was used as the background mixing ratio of CO (Fig. S7S12), which is close to the 0.1 ppm used in Hu et al. (2013) and Yuan et al. (2013). OA/ΔCO was $28.3 \pm 26.3 \mu\text{g m}^{-3} \text{ppmv}^{-1}$ during the studingstudy period, which is comparable to $(41.7 \pm 23.0 \mu\text{g m}^{-3} \text{ppmv}^{-1})$ in suburban Sichuan Basin (Hu et al., 2016) but much lower than the mean value $(70 \pm 20 \mu\text{g m}^{-3} \text{ppmv}^{-1})$ in worldwide urban air (De Gouw and Jimenez, 2009). The scatter plot of OA/ΔCO as a function of O/C ratios during P1C1 and P2EP5 is shown in Fig. 9a10a. Interestingly, different OA/ΔCO variations were found with the increasing O/C during P1C1 and P2EP5. During P1C1, OA/ΔCO ~~trended~~ tended to increase with the increase of the O/C ratio,

420

indicating aging process produced SOA (Hu et al., 2017). In contrast, a remarkable decrease trend of OA/ Δ CO was observed with the increasing O/C during P2EP5, suggesting that less oxidized OA may contribute more significantly to the high OA concentration during this period. Moreover, **considering the cloud evaporation process in this period**, the negative correlation between OA/ Δ CO and O/C in P2EP5 also implies that **more oxidized OA had almost been scavenged by clouds, while the less oxidized OA previously formed or scavenged/**~~incorporated~~ **into cloud droplets was**~~can be~~ **released during cloud evaporation. Another possible mechanism was that after the cloud was evaporated, SOA formation from biogenic VOCs could then be strengthened by stronger solar radiation, which may also contribute to the increase of less oxidized OA. Conversely, more oxidized OA in cloud droplets may have already undergone mass reduction through fragmentation reactions (Lee et al., 2012), which was far less likely to be reintroduced into the atmosphere.** Similarly, significant increases in the LO-OOA concentration (0.27 to 1.70 $\mu\text{g m}^{-3}$) and fraction (40 % to 70 %) were observed from P4C1 to P2EP5, while the MO-OOA concentration (0.40 vs. 0.74 $\mu\text{g m}^{-3}$) did not show large variation (Fig. 9b10b), further supporting our conclusion. **In addition, these released LO-OOA is likely composed of humic like substances (HULIS), which can account for 49 % of the water soluble organic matter at a nearby mountain site in southeastern China (Tao et al., 2023; Chen et al., 2016).**

435

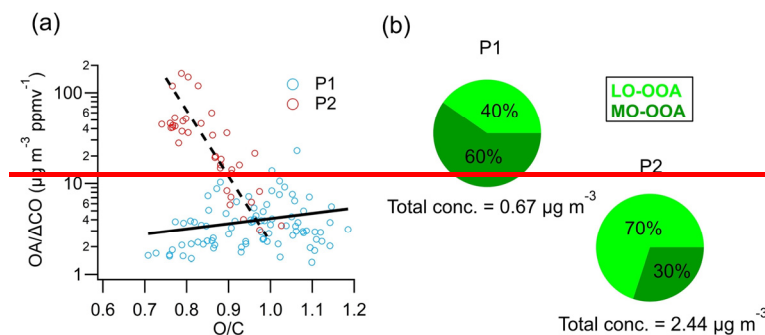


Figure 9. (a) Scatter plot of OA/ Δ CO as a function of O/C ratios and (b) mass concentrations and proportions of MO-OOA and LO-OOA during P1 and P2.

440 **Figure 10a11a** shows the Van Krevelen diagrams of OA in this study ~~together with other mountain sites~~. The slope of H/C to O/C in the present study was -0.66 ($r^2 = 0.64$), **suggesting the addition of carboxyl functional groups during OA evolution (Heald et al., 2010).** ~~This slope is interestingly~~ **slightly flatter than those (-0.7 to mention that -1.0) of other remote/rural regions across the two-OOA factors exhibited a strong alignment with world (Chen et al., 2015), indicating the fitting line, which suggested that the evolution/oxidation processes of OA inat this site likely follows a transformation pathway from LO-OOA to MO-OOA, were more associated with fragmentation reactions.** Consistent evolution trends are also shown in the f_{43} vs. f_{44} space (Fig. 10b11b). The SO_4 -OA and MO-OOA showed similar high ~~oxidative properties~~ **oxidation degrees**, with f_{43} and f_{44} located at the upper part of the triangular region because of the larger fractional contribution of CO_2^+ in the organic

445

mass spectrum. The LO-OOA was situated in the middle region of the triangle, while NIA resided near the bottom right. Moreover, ~~the mass spectra of LO-OOA and MO-OOA both overlapped with resembles to those of~~ the aged OAs observed at other elevated sites (Xu et al., 2018a; Zhou et al., 2019). These results together reveal that OA observed at SH site is representative of the background-aged SOA in the YRD region in China.

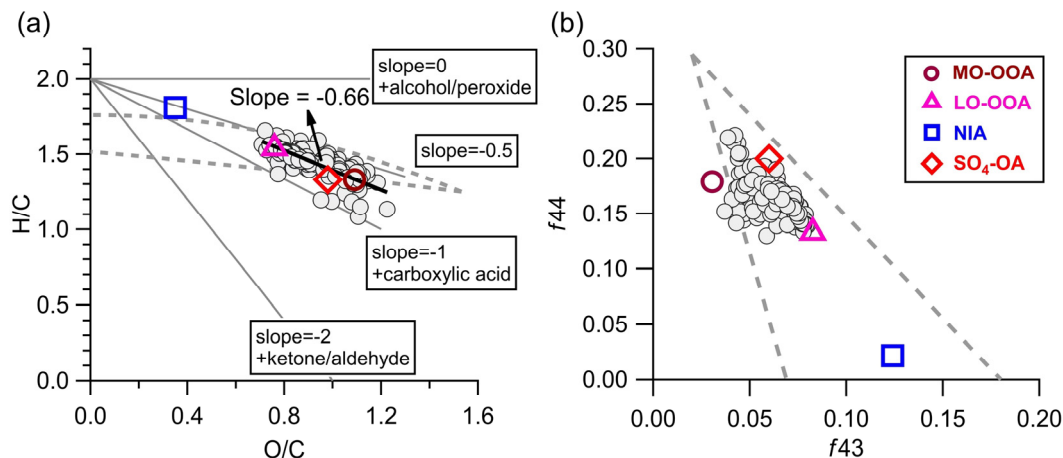
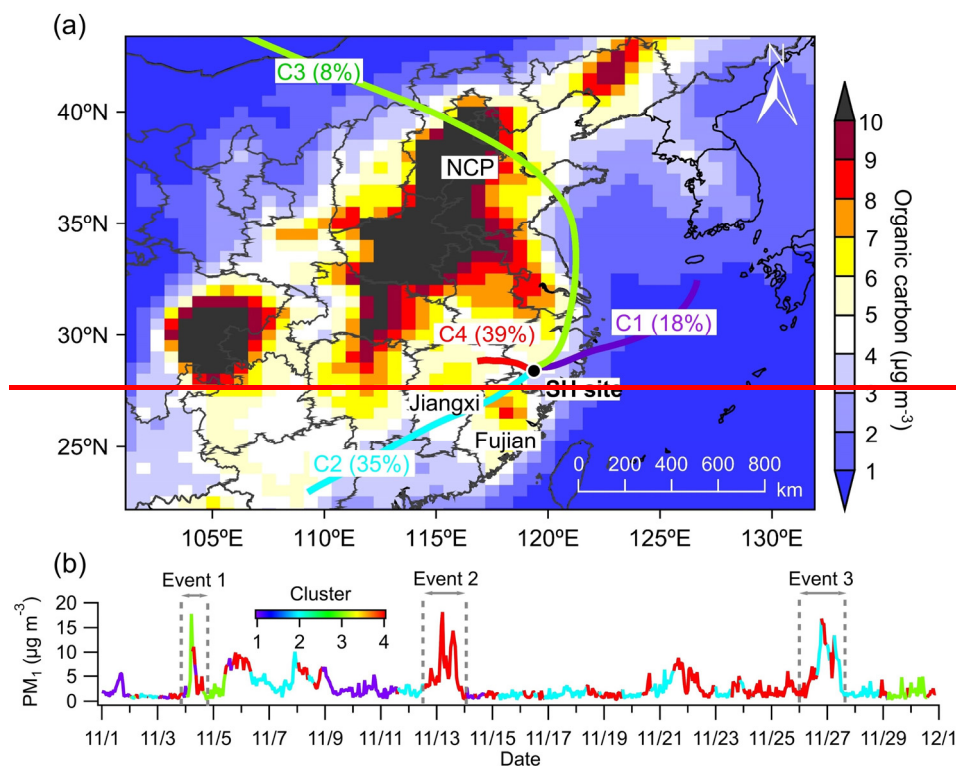


Figure 1011. (a) Van Krevelen diagrams (H/C vs. O/C) and (b) f_{43} vs. f_{44} of OA (grey circles, hourly averaged) and four aerosol factors identified by the PMF analyses during the AMS sampling period.

3.5 Backward trajectory analysis

To explore the potential transport pathway of air mass at this background site, 72 h backward trajectories were calculated for the entire campaign (Fig. 11a). Four air mass clusters were determined, including two clusters from the northeast (C1, C3), one from the southwest (C2), and one from the west (C4). Among the four clusters, C2 and C4 exhibited higher air mass contribution (39 % and 35 %) than the other two clusters (18 % and 8 % for C1 and C3, respectively). According to the surface organic carbon data, these two clusters can bring large amounts of aerosols from Jiangxi and Fujian Province to SH site. This influence of C2 and C4 on the particle concentrations at this site is evident in Fig. 11b, where two PM₁₀ events (Event 2 and 3) were predominantly associated with C2 or C4. These results suggest that the higher levels of PM₁₀ at the SH site may be heavily influenced by the regional transport of air mass from the west and southwest. Additionally, the nitrate event on 4 November (Event 1, discussed in section 3.1) was primarily linked to C3, indicating a potential long distance transport contribution of nitrate particles from the NCP region.



470 **Figure 11.** (a) Average 72 h backward trajectory clusters calculated at 1 h intervals during the entire campaign and (b) temporal variation of 1-hour averaged PM₁ concentration coloured by corresponding clusters.

4 Conclusions

475 ~~The chemical~~Chemical composition and sources of PM₁ ~~were investigated~~ at a forested mountain site in southeastern China in November 2022; ~~were characterized~~ by ~~using~~ two different aerosol mass spectrometers. The average mass concentration of total PM₁ ($4.45 \pm 6.51 \mu\text{g m}^{-3}$) was ~~notably overall~~ lower than those ~~observed~~ at other mountain sites in China, yet ~~it was~~ similarly dominated by ~~OA organics~~ (41.1 %). Remarkably, ~~nitrate (20.9 %) and ammonium (17.0 %) sulfate~~ exhibited ~~unexpectedly high lower~~ contributions (16.7 %) to PM₁ ~~in this forested compared to other~~ mountain ~~area, sites, in contrast to~~ higher contributions of nitrate (14.7%), indicating the ~~impact influences~~ of anthropogenic emissions ~~on clouds and~~ subsequently influencing regional background areas through atmospheric transport. The OA ~~over a relatively small regional scale in southeastern China. Back trajectory analysis revealed that higher concentrations of submicron aerosols at this~~ mountain site were associated with the transport from the western and southwestern regions. OA was ~~primarily of dominantly~~ secondary ~~origin~~ and highly aged, as suggested by the high O/C (0.85–0.96) and OSc (0.21–0.49) ratios. PMF analysis of combined organic and inorganic spectra identified two types of SOA. ~~Notably, OOA and an OA factor associated with SO₄.~~ ~~Most importantly, we found that~~ cloud scavenging and evaporation processes ~~demonstrated differential impacts on influence~~ LO-OOA and MO-OOA. ~~Cloud~~ differently. The cloud scavenging ~~efficiently removed~~ showed a greater efficiency in

485 ~~removing~~ MO-OOA, ~~aligning~~consistent with ~~the~~ smaller size distributions of interstitial particles ~~observed~~ during ~~cloud~~
~~events~~. ~~Conversely~~, cloud ~~events~~. In contrast, ~~the~~ evaporation ~~released a substantial of~~ cloud tended to release a large amount
of LO-OOA, ~~emphasizing~~highlighting that SOA ~~retained~~remained in cloud droplets ~~generally maintained~~was mostly in
a moderate oxidation state. ~~Backward trajectory analysis indicated that higher concentrations of submicron aerosols at the~~
~~mountain site were associated with transport from the western and southwestern regions. In conclusion~~Overall, this study
490 ~~undersees~~illustrates the ~~significance~~importance of SOA in ~~a~~ forested mountain site in southeastern China, where aerosol
concentrations, composition, size distributions, and oxidation ~~states~~state are ~~significantly influenced~~affected by aerosol-
cloud interactions ~~substantially~~. ~~Moreover, our study provides valuable data and insights into understanding the aerosol-~~
~~cloud interactions in mountainous areas that are often under cloudy conditions, and cloud evaporation can be considered as a~~
plausible mechanism to explain certain aerosol episodes in these regions.

495 **Data availability.** Data used in this study can be accessed at repository under: <https://doi.org/10.5281/zenodo.10312334>
(Zhang et al., 2023).

Author contribution. WX and YS designed the research. WX, WZ, and HQ conducted the measurements. ZZ, YZ, WZ, XX,
AD, YZ, XC and YS analysed the data. YK, XP, ZW, LL, QF, DRW, and YS reviewed and commented on the paper. ZZ
and YS wrote the paper.

500 **Competing interests.** DRW is the manufacturer of AMS and ACSM in this study.

utilized in this study. The authors declare that they have no conflict of interest.

Acknowledgements. This work was supported by the National Key Research and Development Program of China (~~No.~~
2022YFC3703500), the Strategic Priority Research Program of the Chinese Academy of Sciences (XDB0760200), and the
National Natural Science Foundation of China (~~No.~~ 42377101).

505 **References**

- Asmi, E., Freney, E., Hervo, M., Picard, D., Rose, C., Colomb, A., and Sellegri, K., Aerosol cloud activation in summer and
winter at puy-de-Dôme high altitude site in France. *Atmos. Chem. Phys.*, 12(23), 11589-607, <https://doi.org/10.5194/acp-12-11589-2012>, 2012.
- 510 Ayres, B. R., Allen, H. M., Draper, D. C., Brown, S. S., Wild, R. J., Jimenez, J. L., Day, D. A., Campuzano-Jost, P., Hu, W.,
de Gouw, J., Koss, A., Cohen, R. C., Duffey, K. C., Romer, P., Baumann, K., Edferton, E., Takahama, S., Thornton, J. A.,
Lee, B. H., Lopez-Hilfiker, F. D., Mohr, C., Wennberg, P. O., Nguyen, T. B., Teng, A., Goldstein, A. H., Olson, K., and
Fry, J. L.: Organic nitrate aerosol formation via NO₃ + biogenic volatile organic compounds in the southeastern United
States. *Atmos. Chem. Phys.*, 15(23), 13377-92, <https://doi.org/10.5194/acp-15-13377-2015>, 2015.

- 515 [Brown, S. S., Ryerson, T. B., Wollny, A. G., Brock, C. A., Peltier, R., Sullivan, A. P., Weber, R. J., Dubé, W. P., Trainer, M., Meagher, J. F., Fehsenfeld, F. C., and Ravishankara, A. R.: Variability in Nocturnal Nitrogen Oxide Processing and Its Role in Regional Air Quality. *Science*, 311\(5757\), 67-70, <https://doi.org/10.1126/science.1120120>, 2006.](#)
- Calvo, A. I., Alves, C., Castro, A., Pont, V., Vicente, A. M., and Fraile, R.: Research on aerosol sources and chemical composition: Past, current and emerging issues, *Atmos. Res.*, 120-121, 1-28, <https://doi.org/10.1016/j.atmosres.2012.09.021>, 2013.
- 520 [Canagaratna, M. R., Jayne, J. T., Jimenez, J. L., Allan, J. D., Alfarra, M. R., Zhang, Q., Onasch, T. B., Drewnick, F., Coe, H., Middlebrook, A., Delia, A., Williams, L. R., Trimborn, A. M., Northway, M. J., DeCarlo, P. F., Kolb, C. E., Davidovits, P., and Worsnop, D. R.: Chemical and microphysical characterization of ambient aerosols with the aerodyne aerosol mass spectrometer. *Mass Spectrom. Rev.*, 26\(2\), 185-222, <https://doi.org/10.1002/mas.20115>, 2007.](#)
- [Canagaratna, M. R., Jimenez, J. L., Kroll, J. H., Chen, Q., Kessler, S. H., Massoli, P., Hildebrandt Ruiz, L., Fortner, E.,](#)
525 [Williams, L. R., Wilson, K. R., Surratt, J. D., Donahue, N. M., Jayne, J. T., and Worsnop, D. R.: Elemental ratio measurements of organic compounds using aerosol mass spectrometry: characterization, improved calibration, and implications, *Atmos. Chem. Phys.*, 15, 253-272, <https://doi.org/10.5194/acp-15-253-2015>, 2015.](#)
- [Cao, L.-M., Wei, J., He, L.-Y., Zeng, H., Li, M.-L., Zhu, Q., Yu, G. H., and Huang, X. F.: Aqueous aging of secondary organic aerosol coating onto black carbon: Insights from simultaneous L-ToF-AMS and SP-AMS measurements at an urban site in southern China. *J. Clean. Prod.*, 330, 129888, <https://doi.org/10.1016/j.jclepro.2021.129888>, 2022.](#)
- 530 [Carbone, C., Decesari, S., Paglione, M., Giulianelli, L., Rinaldi, M., Marinoni, A., Cristofanelli, P., Didiodato, A., Bonasoni, P., Fuzzi, S., and Facchini, M. C.: 3-year chemical composition of free tropospheric PM1 at the Mt. Cimone GAW global station – South Europe – 2165 m a.s.l, ~~*Atmospheric Environment*~~, *Atmos. Environ.*, 87, 218-227, <https://doi.org/10.1016/j.atmosenv.2014.01.048>, 2014.](#)
- 535 [Chen, Q., Heald, C. L., Jimenez, J. L., Canagaratna, M. R., Zhang, Q., He, L.-Y., Huang, X.-F., Campuzano-Jost, P., Palm, B. B., Poulain, L., Kuwara, M., Martin, S. T., ~~Chakraborty~~, Abbatt, J. P. D., Lee, A. K. Y., and Liggio, J.: Elemental composition of organic aerosol: The gap between ambient and laboratory measurements. *Geophys. Res. Lett.*, 42\(10\), 4182-9, <https://doi.org/10.1002/2015GL063693>, 2015.](#)
- ~~[A., Gupta, T., and Tripathi, S. N.: Combined effects of organic aerosol loading and fog processing on organic aerosols oxidation, composition, and evolution, *Sci. Total Environ.*, 573, 690-698, <https://doi.org/10.1016/j.scitotenv.2016.08.156>, 2016.](#)~~
- ~~[Chen, C. L., Chen, T. Y., Hung, H. M., Tsai, P. W., Chou, C. C. K., and Chen, W. N.: The influence of upslope fog on hygroscopicity and chemical composition of aerosols at a forest site in Taiwan, *Atmospheric Environment*, 246, 118150, <https://doi.org/10.1016/j.atmosenv.2020.118150>, 2021.](#)~~
- 545 [Chen, Q., Ikemori, F., Higo, H., Asakawa, D., and Mochida, M.: Chemical Structural Characteristics of HULIS and Other Fractionated Organic Matter in Urban Aerosols: Results from Mass Spectral and FT-IR Analysis, *Environmental Science & Technology*, 50, 1721-1730, \[10.1021/acs.est.5b05277\]\(https://doi.org/10.1021/acs.est.5b05277\), 2016.](#)

- Chen, Y., Xu, L., Humphry, T., Hettiyadura, A. P. S., Ovadnevaite, J., Huang, S., Poulain, L., Schroder, J. C., Campuzano-Jost, P., Jimenez, J. L., Herrmann, H., O'Dowd, C., Stone, E. A., and Ng, N. L.: Response of the Aerodyne Aerosol Mass Spectrometer to Inorganic Sulfates and Organosulfur Compounds: Applications in Field and Laboratory Measurements, *Environ. Sci. Technol.*, 53, 5176-5186, <https://doi.org/10.1021/acs.est.9b00884>, 2019.
- De Gouw, J. and Jimenez, J. L.: Organic Aerosols in the Earth's Atmosphere, *Environ. Sci. Technol.*, 43, 7614-7618, <https://doi.org/10.1021/es9006004>, 2009.
- ~~DeCarlo, P. F., Ulbrich, I. M., Crouse, J., de Foy, B., Dunlea, E. J., Aiken, A. C., Knapp, D., Weinheimer, A. J., Campos, T., Wennberg, P. O., and Jimenez, J. L.: Investigation of the sources and processing of organic aerosol over the Central Mexican Plateau from aircraft measurements during MILAGRO. *Atmos. Chem. Phys.*, 10(12), 5257-80, <https://doi.org/10.5194/acp-10-5257-2010>, 2010.~~
- Ding, S., Liu, D., Hu, K., Zhao, D., Tian, P., Wang, F., Li, R., Chen, Y., He, H., Huang, M., and Ding, D.: Optical and hygroscopic properties of black carbon influenced by particle microphysics at the top of the anthropogenically polluted boundary layer, *Atmos. Chem. Phys.*, 21, 681-694, <https://doi.org/10.5194/acp-21-681-2021>, 2021.
- Du, W., Sun, Y. L., Xu, Y. S., Jiang, Q., Wang, Q. Q., Yang, W., Wang, F., Bai, Z. P., Zhao, X. D., and Yang, Y. C.: Chemical characterization of submicron aerosol and particle growth events at a national background site (3295 m a.s.l.) on the Tibetan Plateau, *Atmos. Chem. Phys.*, 15, 10811-10824, <https://doi.org/10.5194/acp-15-10811-2015>, 2015.
- ~~Fanourgakis, G. S., Kanakidou, M., Nenes, A., Bauer, S. E., Bergman, T., Carslaw, K. S., Grini, A., Hamilton, D. S., Johnson, J. S., Karydis, V. A., Kirkevåg, A., Kodros, J. K., Lohmann, U., Luo, G., Makkonen, R., Matsui, H., Neubauer, D., Pierce, J. R., Schmale, J., Stier, P., Tsigaridis, K., van Noije, T., Wang, H., Watson Parris, D., Westervelt, D. M., Yang, Y., Yoshioka, M., Daskalakis, N., Decesari, S., Gysel Beer, M., Kalivitis, N., Liu, X., Mahowald, N. M., Myriokefalitakis, S., Schrödner, R., Sfakianaki, M., Tsimpidi, A. P., Wu, M., and Yu, F.: Evaluation of global simulations of aerosol particle and cloud condensation nuclei number, with implications for cloud droplet formation, *Atmos. Chem. Phys.*, 19, 8591-8617, [10.5194/acp-19-8591-2019](https://doi.org/10.5194/acp-19-8591-2019), 2019.~~
- Farmer, D. K., Matsunaga, A., Docherty, K. S., Surratt, J. D., Seinfeld, J. H., Ziemann, P. J., and Jimenez, J. L.: Response of an aerosol mass spectrometer to organonitrates and organosulfates and implications for atmospheric chemistry, *P. Natl. Acad. Sci. Proceedings of the National Academy of Sciences USA*, 107, 6670-6675, <https://doi.org/10.1073/pnas.0912340107>, 2010.
- Fry, J. L., Kiendler-Scharr, A., Rollins, A. W., Wooldridge, P. J., Brown, S. S., Fuchs, H., Dubé, W., Mensah, A., dal Maso, M., Tillmann, R., Dorn, H. P., Brauers, T., and Cohen, R. C.: Organic nitrate and secondary organic aerosol yield from NO_3 oxidation of β -pinene evaluated using a gas-phase kinetics/aerosol partitioning model, *Atmos. Chem. Phys.*, 9, 1431-1449, <https://doi.org/10.5194/acp-9-1431-2009>, 2009.
- Fry, J. L., Draper, D. C., Zarzana, K. J., Campuzano-Jost, P., Day, D. A., Jimenez, J. L., Brown, S. S., Cohen, R. C., Kaser, L., Hansel, A., Cappellin, L., Karl, T., Hodzic Roux, A., Turnipseed, A., Cantrell, C., Lefer, B. L., and Grossberg, N.:

- Observations of gas- and aerosol-phase organic nitrates at BEACHON-RoMBAS 2011, *Atmos. Chem. Phys.*, 13, 8585-8605, <https://doi.org/10.5194/acp-13-8585-2013>, 2013.
- Gao, M., Zhou, S. Z., He, Y., Zhang, G. H., Ma, N., Li, Y., Li, F. H., Yang, Y. X., Peng, L., Zhao, J., Bi, X. H., Hu, W. W., Sun, Y. L., Wang, B. G., and Wang, X. M.: In Situ Observation of Multiphase Oxidation-Driven Secondary Organic Aerosol Formation during Cloud Processing at a Mountain Site in Southern China, *Environ. Sci. Technol. Lett.*, 10, 573-581, <https://doi.org/10.1021/acs.estlett.3c00331>, 2023.
- Ge, X. L., Zhang, Q., Sun, Y. L., Ruehl, C. R., and Setyan, A.: Effect of aqueous-phase processing on aerosol chemistry and size distributions in Fresno, California, during wintertime, *Environmental Chemistry, Environ. Chem.*, 9, 221-235, 2012.
- Gelaro, R., McCarty, W., Suárez, M. J., Todling, R., Molod, A., Takacs, L., Randles, C. A., Darmenov, A., Bosilovich, M. G., Reichle, R., Wargan, K., Coy, L., Cullather, R., Draper, C., Akella, S., Buchard, V., Conaty, A., de Silva, A. M., Gu, W., Kim, G.-K., Koster, R., Merkova, D., Nielsen, J. E., Partyka, G., Pawson, S., Putman, W., Rienecker, W., Rienecker, M., Schubert, S. D., Sienkiewicz, M., and Zhao, B.: The Modern-Era Retrospective Analysis for Research and Applications, Version 2 (MERRA-2). *J. Climate*, 30(14), 5419-54, <https://doi.org/10.1175/JCLI-D-16-0758.1>, 2017.
- Gilardoni, S., Massoli, P., Giulianelli, L., Rinaldi, M., Paglione, M., Pollini, F., Lanconelli, C., Poluzzi, V., Carbone, S., Hillamo, R., Russell, L. M., Facchini, M. C., and Fuzzi, S.: Fog scavenging of organic and inorganic aerosol in the Po Valley, *Atmos. Chem. Phys.*, 14, 6967-6981, <https://doi.org/10.5194/acp-14-6967-2014>, 2014.
- Hallquist, M., Wenger, J. C., Baltensperger, U., Rudich, Y., Simpson, D., Claeys, M., Dommen, J., Donahue, N. M., George, C., Goldstein, A. H., Hamilton, J. F., Herrmann, H., Hoffmann, T., Iinuma, Y., Jang, M., Jenkin, M. E., Jimenez, J. L., Kiendler-Scharr, A., Maenhaut, W., McFiggans, G., Mentel, T. F., Monod, A., Prevot, A. S. H., Seinfeld, J. H., Surratt, J. D., Szmigielski, R., and Wildt, J.: The formation, properties and impact of secondary organic aerosol: current and emerging issues, *Atmos. Chem. Phys.*, 9, 5155-5236, <https://doi.org/10.5194/acp-9-5155-2009>, 2009.
- Hao, L. Q., Kortelainen, A., Romakkaniemi, S., Portin, H., Jaatinen, A., Leskinen, A., Komppula, M., Miettinen, P., Sueper, D., Pajunoja, A., Smith, J. N., Lehtinen, K. E. J., Worsnop, D. R., Laaksonen, A., and Virtanen, A.: Atmospheric submicron aerosol composition and particulate organic nitrate formation in a boreal forestland-urban mixed region, *Atmos. Chem. Phys.*, 14, 13483-13495, <https://doi.org/10.5194/acp-14-13483-2014>, 2014.
- Haywood, J. and Boucher, O.: Estimates of the direct and indirect radiative forcing due to tropospheric aerosols: A review, *Reviews of Geophysics, Rev. Geophys.*, 38, 513-543, <https://doi.org/10.1029/1999rg000078>, 2000.
- Heald, C. L., Kroll, J. H., Jimenez, J. L., Docherty, K. S., DeCarlo, P. F., Aiken, A. C., Chen, Q., Martin, S. T., Farmer, D. K., and Artaxo, P.: A simplified description of the evolution of organic aerosol composition in the atmosphere, *Geophys. Res. Lett.*, 37, <https://doi.org/10.1029/2010GL042737>, 2010.
- Hu, W., Hu, M., Hu, W. W., Zheng, J., Chen, C., Wu, Y., and Guo, S.: Seasonal variations in high time-resolved chemical compositions, sources, and evolution of atmospheric submicron aerosols in the megacity Beijing, *Atmos. Chem. Phys.*, 17, 9979-10000, <https://doi.org/10.5194/acp-17-9979-2017>, 2017.

- Hu, W., Hu, M., Hu, W. W., Niu, H., Zheng, J., Wu, Y., Chen, W., Chen, C., Li, L., Shao, M., Xie, S., and Zhang, Y.:
615 Characterization of submicron aerosols influenced by biomass burning at a site in the Sichuan Basin, southwestern China,
Atmos. Chem. Phys., 16, 13213-13230, <https://doi.org/10.5194/acp-16-13213-2016>, 2016.
- Hu, W. W., Hu, M., Yuan, B., Jimenez, J. L., Tang, Q., Peng, J. F., Hu, W., Shao, M., Wang, M., Zeng, L. M., Wu, Y. S.,
Gong, Z. H., Huang, X. F., and He, L. Y.: Insights on organic aerosol aging and the influence of coal combustion at a
regional receptor site of central eastern China, Atmos. Chem. Phys., 13, 10095-10112, 10.5194/acp-13-10095-2013, 2013.
- 620 Huang, R. J., Zhang, Y. L., Bozzetti, C., Ho, K. F., Cao, J. J., Han, Y. M., Daellenbach, K. R., Slowik, J. G., Platt, S. M.,
Canonaco, F., Zotter, P., Wolf, R., Pieber, S. M., Bruns, E. A., Crippa, M., Ciarelli, G., Piazzalunga, A., Schwikowski, M.,
Abbaszade, G., Schnelle-Kreis, J., Zimmermann, R., An, Z. S., Szidat, S., Baltensperger, U., El Haddad, I., and Prevot, A.
S. H.: High secondary aerosol contribution to particulate pollution during haze events in China, Nature, 514, 218-222,
<https://doi.org/10.1038/nature13774>, 2014.
- 625 Huang, W., Yang, Y., Wang, Y. H., Gao, W. K., Li, H. Y., Zhang, Y. Y., Li, J. Y., Zhao, S. M., Yan, Y. C., Ji, D. S., Tang,
G. Q., Liu, Z. R., Wang, L. L., Zhang, R. J., and Wang, Y. S.: Exploring the inorganic and organic nitrate aerosol
formation regimes at a suburban site on the North China Plain, Sci. Total Environ., 768, 144538,
<https://doi.org/10.1016/j.scitotenv.2020.144538>, 2021.
- Huang, X., Ding, A. J., Wang, Z. L., Ding, K., Gao, J., Chai, F. H., and Fu, C. B.: Amplified transboundary transport of haze
630 by aerosol-boundary layer interaction in China, Nat. Geosci., 13, 428 ~~+~~, 434, <https://doi.org/10.1038/s41561-020-0583-4>,
2020.
- Kampa, M. and Castanas, E.: Human health effects of air pollution, Environmental Pollution, Environ. Pollut., 151, 362-367,
<https://doi.org/10.1016/j.envpol.2007.06.012>, 2008.
- Kanakidou, M., Seinfeld, J. H., Pandis, S. N., Barnes, I., Dentener, F. J., Facchini, M. C., Van Dingenen, R., Ervens, B.,
635 Nenes, A., Nielsen, C. J., Swietlicki, E., Putaud, J. P., Balkanski, Y., Fuzzi, S., Horth, J., Moortgat, G. K., Winterhalter, R.,
Myhre, C. E. L., Tsigaridis, K., Vignati, E., Stephanou, E. G., and Wilson, J.: Organic aerosol and global climate
modelling: a review, Atmos. Chem. Phys., 5, 1053-1123, <https://doi.org/10.5194/acp-5-1053-2005>, 2005.
- KimKuang, Y., Xu, W., Tao, J., Luo, B., Liu, L., Xu, H., Collier, S., Ge, X., Xu, J., Xu, W., Xue, B., Zhai, M., Liu, P., and
Sun, Y., Jiang, W., Wang, Y.: Divergent Impacts of Biomass Burning and Fossil Fuel Combustion Aerosols on Fog-Cloud
640 Microphysics and Chemistry: Novel Insights From Advanced Aerosol-Fog Sampling, Geophys. Res. Lett., 51,
e2023GL107147, https://doi.org/10.1029/2023GL107147, 2024.
- Lee, A. K. Y., Hayden, K. L., Herckes, P., and Zhang, Q.: Chemical processing of Leaitch, W. R., Liggio, J., Macdonald, A.
M., and Abbatt, J. P. D.: Characterization of aerosol and cloud water-soluble species and formation of
during WACS 2010: secondary organic aerosol in fogs, Atmospheric Environment, 200, 158-166
645 formation through
oxidative cloud processing. Atmos. Chem. Phys., 12(15), 7103-16, https://doi.org/10.4016/j.atmosenv.2018.11.062,
20195194/acp-12-7103-2012.

- Li, J. J., Wang, G. H., Cao, J. J., Wang, X. M., and Zhang, R. J.: Observation of biogenic secondary organic aerosols in the atmosphere of a mountain site in central China: temperature and relative humidity effects, *Atmos. Chem. Phys.*, 13, 11535-11549, <https://doi.org/10.5194/acp-13-11535-2013>, 2013.
- 650 [Li, Z. Y., Xie, P. H., Hu, R. Z., Wang, D., Jin, H. W., Chen, H., Lin, C., and Liu, W. Q.: Observations of N₂O₅ and NO₃ at a suburban environment in Yangtze river delta in China: Estimating heterogeneous N₂O₅ uptake coefficients. *J. Environ. Sci.*, 95, 248-55, <https://doi.org/10.1016/j.jes.2020.04.041>, 2020.](https://doi.org/10.1016/j.jes.2020.04.041)
- Lin, C., Huang, R.-J., Duan, J., Zhong, H., and Xu, W.: Primary and Secondary Organic Nitrate in Northwest China: A Case Study, *Environ. Sci. Technol. Lett.*, 8, 947-953, <https://doi.org/10.1021/acs.estlett.1c00692>, 2021.
- 655 Middlebrook, A. M., Bahreini, R., Jimenez, J. L., and Canagaratna, M. R.: Evaluation of Composition-Dependent Collection Efficiencies for the Aerodyne Aerosol Mass Spectrometer using Field Data, *Aerosol Science and Technology*, 46, 258-271, <https://doi.org/10.1080/02786826.2011.620041>, 2012.
- Monks, P. S., Granier, C., Fuzzi, S., Stohl, A., Williams, M. L., Akimoto, H., Amann, M., Baklanov, A., Baltensperger, U., Bey, I., Blake, N., Blake, R. S., Carslaw, K., Cooper, O. R., Dentener, F., Fowler, D., Fragkou, E., Frost, G. J., Generoso, 660 S., Ginoux, P., Grewe, V., Guenther, A., Hansson, H. C., Henne, S., Hjorth, J., Hofzumahaus, A., Huntrieser, H., Isaksen, I. S. A., Jenkin, M. E., Kaiser, J., Kanakidou, M., Klimont, Z., Kulmala, M., Laj, P., Lawrence, M. G., Lee, J. D., Liousse, C., Maione, M., McFiggans, G., Metzger, A., Mieville, A., Moussiopoulos, N., Orlando, J. J., O'Dowd, C. D., Palmer, P. I., Parrish, D. D., Petzold, A., Platt, U., Pöschl, U., Prévôt, A. S. H., Reeves, C. E., Reimann, S., Rudich, Y., Sellegri, K., Steinbrecher, R., Simpson, D., ten Brink, H., Theloke, J., van der Werf, G. R., Vautard, R., Vestreng, V., Vlachokostas, C., 665 and von Glasow, R.: Atmospheric composition change – global and regional air quality, *Atmospheric Environment*, 43, 5268-5350, <https://doi.org/10.1016/j.atmosenv.2009.08.021>, 2009.
- [Nault, B. A., Croteau, P., Jayne, J., Williams, A., Williams, L., Worsnop, D. R., Katz, E. F., DeCarlo, P. F., and Canagaratna, M.: Laboratory evaluation of organic aerosol relative ionization efficiencies in the aerodyne aerosol mass spectrometer and aerosol chemical speciation monitor. *Aerosol Sci. Technol.*, 57\(10\), 981-97, <https://doi.org/10.1080/02786826.2023.2223249>, 2023.](https://doi.org/10.1080/02786826.2023.2223249)
- 670 Pokorná, P., Zíková, N., Vodička, P., Lhotka, R., Mbengue, S., Holubová Šmejkalová, A., Riffault, V., Ondráček, J., Schwarz, J., and Ždímal, V.: Chemically speciated mass size distribution, particle density, shape and origin of non-refractory PM₁ measured at a rural background site in central Europe, *Atmos. Chem. Phys.*, 22, 5829-5858, <https://doi.org/10.5194/acp-22-5829-2022>, 2022.
- 675 Ramanathan, V., Crutzen, P. J., Kiehl, J. T., and Rosenfeld, D.: Atmosphere - Aerosols, climate, and the hydrological cycle, *Science*, 294, 2119-2124, <https://doi.org/10.1126/science.1064034>, 2001.
- [Rejano, F., Titos, G., Casquero-Vera, J. A., Lyamani, H., Andrews, E., Sheridan, P., Cazorla, A., Castillo, S., Alados-Arboledas, L., and Olmo, F.: Activation properties of aerosol particles as cloud condensation nuclei at urban and high-altitude remote sites in southern Europe. *Sci. Tot. Environ.*, 762, 143100, <https://doi.org/10.1016/j.scitotenv.2020.143100>, 680 \[2021\]\(https://doi.org/10.1016/j.scitotenv.2020.143100\).](https://doi.org/10.1016/j.scitotenv.2020.143100)

- Roth, A., Schneider, J., Klimach, T., Mertes, S., van Pinxteren, D., Herrmann, H., and Borrmann, S.: Aerosol properties, source identification, and cloud processing in orographic clouds measured by single particle mass spectrometry on a central European mountain site during HCCT-2010. *Atmos Chem Phys.*, 16(2), 505-24, <https://doi.org/10.5194/acp-16-505-2016>, 2016.
- 685 Song, S. J., Gao, M., Xu, W. Q., Sun, Y. L., Worsnop, D. R., Jayne, J. T., Zhang, Y. Z., Zhu, L., Li, M., Zhou, Z., Cheng, C. L., Lv, Y. B., Wang, Y., Peng, W., Xu, X. B., Lin, N., Wang, Y. X., Wang, S. X., Munger, J. W., Jacob, D. J., and McElroy, M. B.: Possible heterogeneous chemistry of hydroxymethanesulfonate (HMS) in northern China winter haze, *Atmos. Chem. Phys.*, 19, 1357-1371, <https://doi.org/10.5194/acp-19-1357-2019>, 2019.
- ~~Sun, Y., Wang, Z., Fu, P., Jiang, Q., Yang, T., Li, J., and Ge, X.: The impact of relative humidity on aerosol composition and evolution — processes — during — wintertime — in — Beijing, — China, — Atmospheric — Environment, — 77, — 927-934, <https://doi.org/10.1016/j.atmosenv.2013.06.019>, 2013.~~
- 690 Sun, Y. L., Zhang, Q., Schwab, J. J., Yang, T., Ng, N. L., and Demerjian, K. L.: Factor analysis of combined organic and inorganic aerosol mass spectra from high resolution aerosol mass spectrometer measurements, *Atmos. Chem. Phys.*, 12, 8537-8551, <https://doi.org/10.5194/acp-12-8537-2012>, 2012.
- 695 Sun, Y. L., Zhang, Q., Schwab, J. J., Chen, W. N., Bae, M. S., Lin, Y. C., Hung, H. M., and Demerjian, K. L.: A case study of aerosol processing and evolution in summer in New York City, *Atmos. Chem. Phys.*, 11, 12737-12750, <https://doi.org/10.5194/acp-11-12737-2011>, 2011.
- Tang, C. G., Zhang, X. H., Tian, P. F., Guan, X., Lin, Y. J., Pang, S. T., Guo, Q., Du, T., Zhang, Z. D., Zhang, M., Xu, J. Z., and Zhang, L.: Chemical characteristics and regional transport of submicron particulate matter at a suburban site near Lanzhou, China, *Environ. Res.*, 212, 113179, <https://doi.org/10.1016/j.envres.2022.113179>, 2022.
- 700 Tang, L. L., Yu, H. X., Ding, A. J., Zhang, Y. J., Qin, W., Wang, Z., Chen, W. T., Hua, Y., and Yang, X. X.: Regional contribution to PM₁ pollution during winter haze in Yangtze River Delta, China, *Sci. Total Environ.*, 541, 161-166, <https://doi.org/10.1016/j.scitotenv.2015.05.058>, 2016.
- Tao, J., Zhang, Z. S., Tan, H. B., Zhang, L. M., Wu, Y. F., Sun, J. R., Che, H. Z., Cao, J. J., Cheng, P., Chen, L. G., and Zhang, R. J.: Observational evidence of cloud processes contributing to daytime elevated nitrate in an urban atmosphere, ~~*Atmospheric Environment*~~, *Atmos. Environ.*, 186, 209-215, <https://doi.org/10.1016/j.atmosenv.2018.05.040>, 2018.
- ~~Tao, J., Zhang, Z., Zhang, L., Wu, Y., Ren, Y., Li, J., Huang, J., Wang, G., Shen, Z., Zhang, R., and Wang, B.: Characterization and sources of water-soluble organic species in PM_{2.5} in a remote mountain environment in Southeastern China, *Atmospheric Environment*, 313, 120057, <https://doi.org/10.1016/j.atmosenv.2023.120057>, 2023.~~
- 710 ~~Timonen, H., Wigder, N., and Jaffe, D.: Influence of background particulate matter. (PM) on urban air quality in the Pacific Northwest, *Journal of Environmental Management*, 129, 333-340, <https://doi.org/10.1016/j.jenvman.2013.07.023>, 2013.~~
- Ulbrich, I. M., Canagaratna, M. R., Zhang, Q., Worsnop, D. R., and Jimenez, J. L.: Interpretation of organic components from Positive Matrix Factorization of aerosol mass spectrometric data, *Atmos. Chem. Phys.*, 9, 2891-2918, <https://doi.org/10.5194/acp-9-2891-2009>, 2009.

- 715 Wang, J. F., Ge, X. L., Chen, Y. F., Shen, Y. F., Zhang, Q., Sun, Y. L., Xu, J. Z., Ge, S., Yu, H., and Chen, M. D.: Highly time-resolved urban aerosol characteristics during springtime in Yangtze River Delta, China: insights from soot particle aerosol mass spectrometry, *Atmos. Chem. Phys.*, 16, 9109-9127, <https://doi.org/10.5194/acp-16-9109-2016>, 2016.
- Wang, Q. Y., Huang, R. J., Cao, J. J., Tie, X. X., Ni, H. Y., Zhou, Y. Q., Han, Y. M., Hu, T. F., Zhu, C. S., Feng, T., Li, N., and Li, J. D.: Black carbon aerosol in winter northeastern Qinghai-Tibetan Plateau, China: the source, mixing state and optical property, *Atmos. Chem. Phys.*, 15, 13059-13069, <https://doi.org/10.5194/acp-15-13059-2015>, 2015.
- 720 [Wen, L., Xue, L. K., Dong, C., Wang, X. F., Chen, T. S., Jiang, Y., Gu, R. R., Zheng, P. G., Li, H. Y., Shan, Y., Zhu, Y. J., Zhao, Y., Yin, X. K., Liu, H. D., Gao, J., Wu, Z. J., Wang, T., Herrmann, H., and Wang, W. X.: Reduced atmospheric sulfate enhances fine particulate nitrate formation in eastern China. *Sci. Total Environ.*, 898, 165303, <https://doi.org/10.1016/j.scitotenv.2023.165303>, 2023.](https://doi.org/10.1016/j.scitotenv.2023.165303)
- 725 [Xian, J., Cui, S., Chen, X., Wang, J., Xiong, Y., Gu, C., Wang, Y., Zhang, Y. J., Li, H. W., Wang, J. F., and Ge, X. L.: Online chemical characterization of atmospheric fine secondary aerosols and organic nitrates in summer Nanjing, China. *Atmos. Res.*, 290, 106783, <https://doi.org/10.1016/j.atmosres.2023.106783>, 2023.](https://doi.org/10.1016/j.atmosres.2023.106783)
- Xu, J., Zhang, Q., Chen, M., Ge, X., Ren, J., and Qin, D.: Chemical composition, sources, and processes of urban aerosols during summertime in northwest China: insights from high-resolution aerosol mass spectrometry, *Atmos. Chem. Phys.*, 14, 12593-12611, <https://doi.org/10.5194/acp-14-12593-2014>, 2014.
- 730 Xu, J. Z., Zhang, Q., Shi, J. S., Ge, X. L., Xie, C. H., Wang, J. F., Kang, S. C., Zhang, R. X., and Wang, Y. H.: Chemical characteristics of submicron particles at the central Tibetan Plateau: insights from aerosol mass spectrometry, *Atmos. Chem. Phys.*, 18, 427-443, <https://doi.org/10.5194/acp-18-427-2018>, 2018a.
- [Xu, J., Zhu, F., Wang, S., Zhao, X., Zhang, M., Ge, X., Wang, J., Tian, W., Wang, L., Yang, L., Ding, L., Lu, X., Chen, X., Zheng, Y., and Guo, Z.: Impacts of relative humidity on fine aerosol properties via environmental wind tunnel experiments, *Atmospheric Environment*, 206, 21-29, <https://doi.org/10.1016/j.atmosenv.2019.03.002>, 2019.](https://doi.org/10.1016/j.atmosenv.2019.03.002)
- 735 Xu, L., Suresh, S., Guo, H., Weber, R. J., and Ng, N. L.: Aerosol characterization over the southeastern United States using high-resolution aerosol mass spectrometry: spatial and seasonal variation of aerosol composition and sources with a focus on organic nitrates, *Atmos. Chem. Phys.*, 15, 7307-7336, <https://doi.org/10.5194/acp-15-7307-2015>, 2015.
- 740 Xu, P., Zhang, J. K., Ji, D. S., Liu, Z. R., Tang, G. Q., Jiang, C. S., and Wang, Y. S.: Characterization of submicron particles during autumn in Beijing, China, *Journal of Environmental Sciences, J. Environ. Sci.*, 63, 16-27, <https://doi.org/10.1016/j.jes.2017.03.036>, 2018b.
- [Yu, K., Zhu, Q., Du, K., and Huang, X. F.: Characterization of nighttime formation of particulate organic nitrates based on high-resolution aerosol mass spectrometry in an urban atmosphere in China. *Atmos. Chem. Phys.*, 19\(7\), 5235-49, <https://doi.org/10.5194/acp-19-5235-2019>, 2019.](https://doi.org/10.5194/acp-19-5235-2019)
- 745 Yuan, B., Hu, W. W., Shao, M., Wang, M., Chen, W. T., Lu, S. H., Zeng, L. M., and Hu, M.: VOC emissions, evolutions and contributions to SOA formation at a receptor site in eastern China, *Atmos. Chem. Phys.*, 13, 8815-8832, <https://doi.org/10.5194/acp-13-8815-2013>, 2013.

- Zhang, Q., Jimenez, J. L., Canagaratna, M. R., Ulbrich, I. M., Ng, N. L., Worsnop, D. R., and Sun, Y. L.: Understanding atmospheric organic aerosols via factor analysis of aerosol mass spectrometry: a review, *Analytical and Bioanalytical Chemistry*, *Anal. Bioanal. Chem.*, 401, 3045-3067, <https://doi.org/10.1007/s00216-011-5355-y>, 2011.
- Zhang, X. H., Xu, J. Z., Kang, S. C., Liu, Y. M., and Zhang, Q.: Chemical characterization of long-range transport biomass burning emissions to the Himalayas: insights from high-resolution aerosol mass spectrometry, *Atmos. Chem. Phys.*, 18, 4617-4638, <https://doi.org/10.5194/acp-18-4617-2018>, 2018.
- Zhang, X. H., Xu, J. Z., Kang, S. C., Zhang, Q., and Sun, J. Y.: Chemical characterization and sources of submicron aerosols in the northeastern Qinghai-Tibet Plateau: insights from high-resolution mass spectrometry, *Atmos. Chem. Phys.*, 19, 7897-7911, <https://doi.org/10.5194/acp-19-7897-2019>, 2019.
- Zhang, Y. J., Tang, L. L., Wang, Z., Yu, H. X., Sun, Y. L., Liu, D., Qin, W., Canonaco, F., Prévôt, A. S. H., Zhang, H. L., and Zhou, H. C.: Insights into characteristics, sources, and evolution of submicron aerosols during harvest seasons in the Yangtze River delta region, China, *Atmos. Chem. Phys.*, 15, 1331-1349, <https://doi.org/10.5194/acp-15-1331-2015>, 2015.
- Zhang, J. K., Cheng, M. T., Ji, D. S., Liu, Z. R., Hu, B., Sun, Y. L., Wang, Y. S.: Characterization of submicron particles during biomass burning and coal combustion periods in Beijing, China. *Sci. Total Environ.*, 562, 812-21, <https://doi.org/10.1016/j.scitotenv.2016.04.015>, 2016.
- Zhang, Y. M., Zhang, X. Y., Sun, J. Y., Hu, G. Y., Shen, X. J., Wang, Y. Q., Wang, T. T., Wang, D. Z., and Zhao, Y.: Chemical composition and mass size distribution of PM_{10} at an elevated site in central east China, *Atmos. Chem. Phys.*, 14, 12237-12249, <https://doi.org/10.5194/acp-14-12237-2014>, 2014.
- Zheng, J., Hu, M., Du, Z. F., Shang, D. J., Gong, Z. H., Qin, Y. H., Fang, J. Y., Gu, F. T., Li, M. R., Peng, J. F., Li, J., Zhang, Y. Q., Huang, X. F., He, L. Y., Wu, Y. S., and Guo, S.: Influence of biomass burning from South Asia at a high-altitude mountain receptor site in China, *Atmos. Chem. Phys.*, 17, 6853-6864, <https://doi.org/10.5194/acp-17-6853-2017>, 2017.
- Zhong, H. B., Huang, R. J., Lin, C. S., Xu, W., Duan, J., Gu, Y. F., Huang, W., Ni, H. Y., Zhu, C. S., You, Y., Wu, Y. F., Zhang, R. J., Ovadnevaite, J., Ceburnis, D., and O'Dowd, C. D.: Measurement report: On the contribution of long-distance transport to the secondary aerosol formation and aging, *Atmos. Chem. Phys.*, 22, 9513-9524, <https://doi.org/10.5194/acp-22-9513-2022>, 2022.
- Zhou, S., Collier, S., Jaffe, D. A., and Zhang, Q.: Free tropospheric aerosols at the Mt. Bachelor Observatory: more oxidized and higher sulfate content compared to boundary layer aerosols, *Atmos. Chem. Phys.*, 19, 1571-1585, <https://doi.org/10.5194/acp-19-1571-2019>, 2019.
- Zhou, W., Xu, W. Q., Kim, H., Zhang, Q., Fu, P. Q., Worsnop, D. R., and Sun, Y. L.: A review of aerosol chemistry in Asia: insights from aerosol mass spectrometer measurements, *Environmental Science: Processes & Impacts*, 22, *Environ. Sci.-Proc. Imp.*, 22, <https://doi.org/10.1039/D0EM00212G>, 2020.
- Zhu, Q., He, L. Y., Huang, X. F., Cao, L. M., Gong, Z. H., Wang, C., Zhuang, X., and Hu, M.: Atmospheric aerosol compositions and sources at two national background sites in northern and southern China, *Atmos. Chem. Phys.*, 16, 10283-10297, <https://doi.org/10.5194/acp-16-10283-2016>, 2016.